Journal of Medicinal Chemistry

Article

pubs.acs.org/jmc

Design and Synthesis of Active Site Inhibitors of the Human Farnesyl Pyrophosphate Synthase: Apoptosis and Inhibition of ERK Phosphorylation in Multiple Myeloma Cells

Yih-Shyan Lin,[†] Jaeok Park,[‡] Joris W. De Schutter,[†] Xian Fang Huang,[§] Albert M. Berghuis,[‡] Michael Sebag,[§] and Youla S. Tsantrizos*[,‡,†]

[†]Department of Chemistry, McGill University, 801 Sherbrooke Street West, Montreal, QC, Canada H3A 0B8

[‡]Department of Biochemistry, McGill University, 3649 Promenade Sir William Osler, Montreal, QC, Canada H3G 0B1

[§]Division of Haematology, McGill University Health Center, Royal Victoria Hospital, C6.80, 687 Pine Avenue West, Montreal, QC, Canada H3A 1A1

Supporting Information

ABSTRACT: Human farnesyl pyrophosphate synthase (hFPPS) controls intracellular levels of FPP and post-translational prenylation of small GTPase proteins, which are essential for cell signaling and cell proliferation. Clinical investigations provide evidence that *N*-BP inhibitors of hFPPS are disease modifying agents that improve survival of multiple myeloma (MM) patients via mechanisms unrelated to their skeletal effects. A new series of *N*-BPs was designed that interact with a larger portion of the GPP subpocket, as compared to the current therapeutic drugs, and rigidify the ^{364}KRRK^{367} tail of hFPPS in the closed conformation in the absence of IPP. An analogue of this series was used to demonstrate inhibition of the intended biological target, resulting in apoptosis and down-regulation of ERK phosphorylation in human MM cell lines.

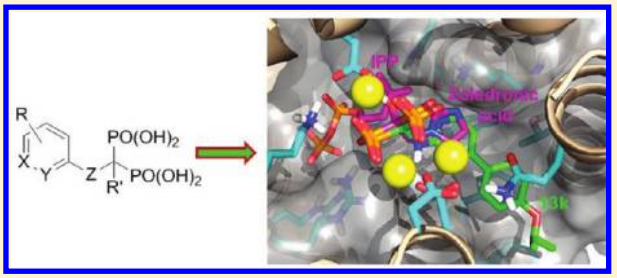

INTRODUCTION

Human farnesyl pyrophosphate synthase (hFPPS) is responsible for the catalytic elongation of dimethylallyl pyrophosphate (DMAPP) to farnesyl pyrophosphate (FPP) via the successive condensation of two isopentenyl pyrophosphate (IPP) units and controls intracellular levels of all downstream isoprenoids, including geranylgeranyl pyrophosphate (GGPP). FPP and GGPP are essential for the post-translational prenylation of small GTPases, a family of signaling proteins that are fundamentally important for cell survival.[1] Farnesylated proteins (e.g., H-Ras, K-Ras, and N-Ras) are predominant in oncogenesis.[1] Recent whole genome sequencing of multiple myeloma (MM) human tumors has shown that 50% of multiple myeloma (MM) patients harbored either K-Ras or N-Ras mutations, underscoring the importance of hFPPS in this disease.[2]

Nitrogen-containing bisphosphonates (*N*-BPs) are the only clinically validated drugs that target hFPPS.[3,4] They are potent inhibitors of osteoclastic activity and are widely used for the treatment of bone-related diseases.[5] Recent clinical investigations provided evidence that *N*-BPs are also disease modifying agents that improve survival in patients with multiple myeloma (MM) via mechanisms unrelated to their skeletal effects.[6] In addition to down-regulating Ras prenylation, intracellular accumulation of IPP leads to the formation of an ATP derivative (ApppI), which induces apoptosis by inhibiting the mitochondrial adenine nucleotide translocase (ANT).[7,8] IPP is also a natural antigen that directly stimulates $\gamma\delta$ T cells carrying the Vγ2 Vδ2 T cell receptors and is strongly implicated in the human innate immune response against tumors and pathogens.[9]

The current *N*-BP drugs are highly polar molecules that exhibit poor cell-membrane permeability and oral bioavailability; consequently their effects in nonskeletal tissues are seriously compromised. Furthermore, their molecular interactions with hFPPS are suboptimal, leaving a large portion of the active site cavity unoccupied.[3,4] Efforts toward improving the clinical usefulness of *N*-BPs have included investigations of ester[10] and peptide pro-drugs,[11] formulations using liposome,[12] and structural modifications. Analogues such as Cα-deoxy (e.g., **9**), Cα-halogenated (e.g., **8**), aminobisphosphonates (e.g., **3**) and analogues with large lipophilic heterocyclic side chains (e.g., **4**), have been explored.[13−19] These studies have demonstrated that even minor structural modifications can compromise the potency and selectivity of *N*-BPs toward hFPPS. Inhibition of structurally related human enzymes by *N*-BPs has been observed with hGGPPS (e.g., **4** and **5**),[16] decaprenyl diphosphate synthase (hDPPS; e.g., **4**),[16,19] and squalene synthase (hSQS; e.g., **6**)[20,21] More recently, non-bisphosphonate inhibitors of hFPPS were identified (e.g., compound **7**) that bind in an allosteric pocket of hFPPS and

Received: December 7, 2011
Published: March 5, 2012

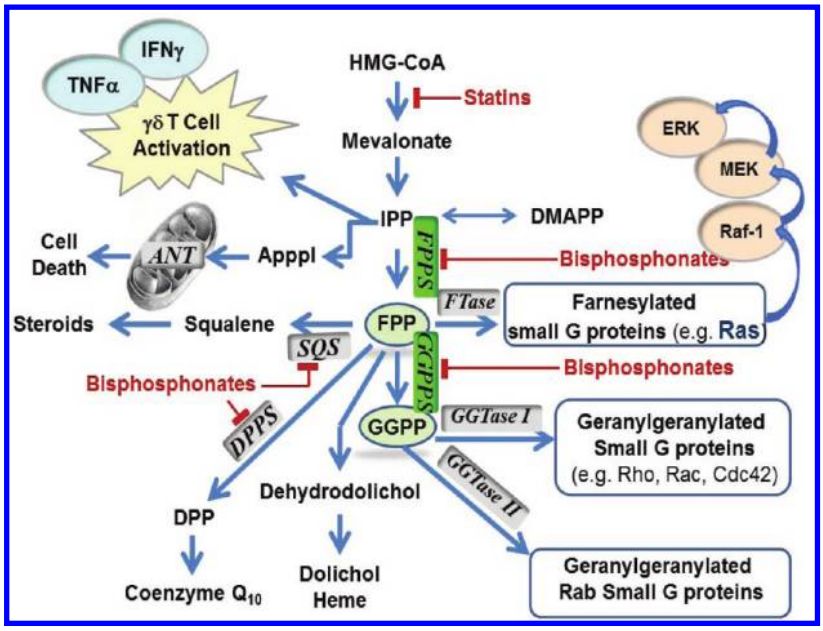

Figure 1. Schematic representation of pathways associated with the biological role of hFPPS. Classes of drugs that modulate the function of hFPPS, statins (indirectly) and bisphosphonates (directly), are indicated (red line). FPPS and GGPS enzymes are highlighted in green boxes; other key enzymes are highlighted in gray boxes.

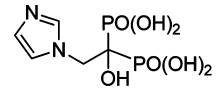

1, Zoledronic acid

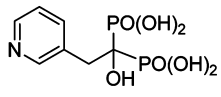

2, Risedronic acid

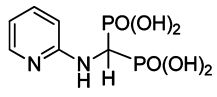

3

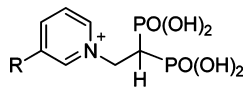

4, R = $O(CH_2)_9CH_3$

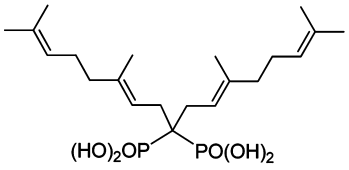

5

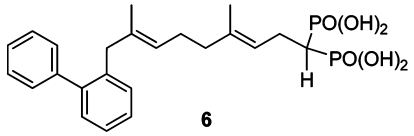

6

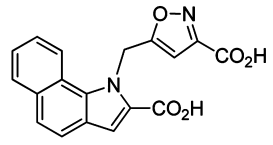

7

sterically hinder the binding of IPP.[22] In spite of all these efforts, the identification of highly potent and selective inhibitors of hFPPS, with good cell membrane permeability and oral bioavailability, remains a daunting challenge.

We reasoned that it may be possible to design molecules with better size, shape, and electrostatic surface complementarity for the active site of hFPPS, as compared to the best current drugs, such as zoledronic acid (**1**) and risedronic acid (**2**), and presumed that these molecules would exhibit high affinity and selectivity for hFPPS. We aimed to design more lipophilic molecules, in order to also improve antitumor activity in MM cells. Herein, we report potent *N*-BP inhibitors of hFPPS with a novel molecular structure. The crystal structure of an inhibitor/hFPPS complex reveals that these analogues interact with a larger portion of the GPP subpocket, as compared to the current therapeutic drugs **1** and **2**, and rigidify the ^{364}KRRK^{367} tail of hFPPS in the closed conformation in the absence of cobound IPP. Analogues from this series are able to inhibit their intended target in MM cells, resulting in apoptosis and inhibition of ERK phosphorylation, downstream of the Ras signaling pathway (Figure 1).

CHEMISTRY

Recently, we reported the identification of a novel series of *N*-BP inhibitors of hFPPS.[23] Our subsequent hit-to-lead optimization efforts focused on the synthesis of compound libraries with structures **8**–**16** (Table 1). Synthetic protocols were modified and rendered amenable to high throughput parallel synthesis. Docking (using GLIDE, version 5.5., Schrödinger, LLC, New York, NY 2009; standard parameters of XP-mode) of virtual molecules to the fully closed hFPPS active site (PDB ID: 1ZW5) was employed to filter poorly binding analogues. The synthesis of **8**–**11** is summarized in Scheme 1.

Synthesis of analogues **8** and **9** (Table 1, Scheme 1) was initiated by the conversion of halonicotinic acids to the corresponding benzylic alcohols and then to the bromides (i.e., analogues of **17**, where Cl is replaced by Br). This three-step conversion was achieved by reacting the starting material with ethylchloroformate (to form the mixed anhydride), followed by reduction of the crude anhydride with $NaBH_4$ to give the alcohol (~50% overall yield). The benzylic alcohol was then treated with PBr_3 to obtain the bromide in good yield (~70%). The benzylic bromides were found to be chemically unstable, leading to modest and inconsistent yields for the subsequent

dx.doi.org/10.1021/jm201657x | J. Med. Chem. 2012, 55, 3201–3215

Table 1. Key Examples from the Compound Library

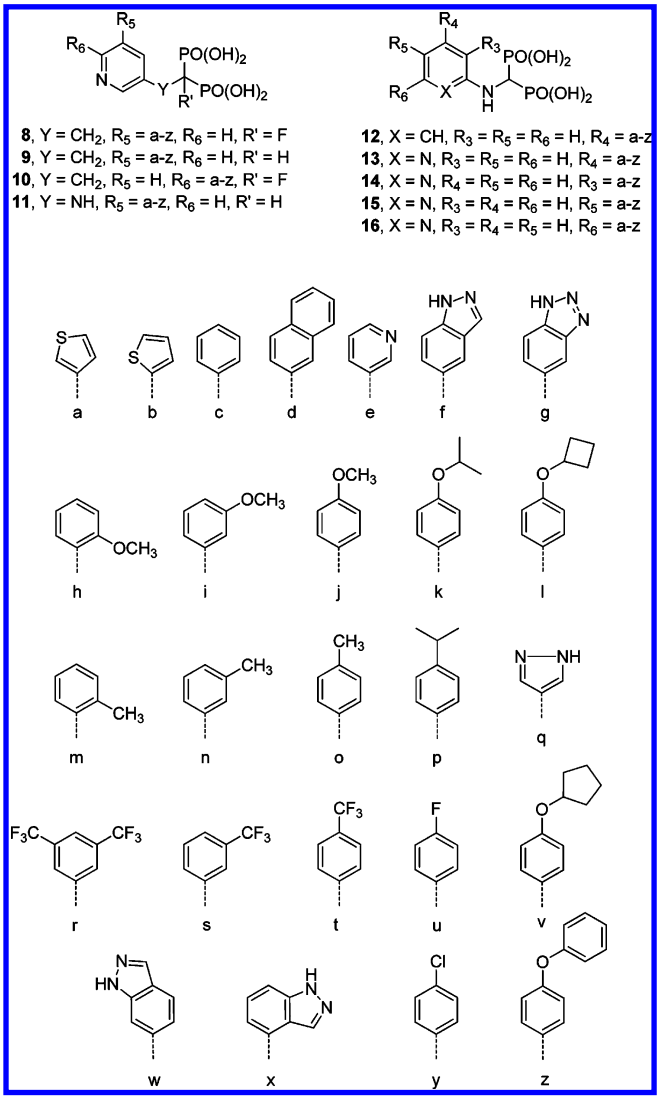

step. To overcome this problem, the benzylic chlorides **17** were prepared and reacted directly with the Cα anion of tetraethyl methylenebis(phosphonate); however, only minor amounts of the desired bisphosphonate products were formed. *In situ* conversion of the chlorides **17** to the corresponding iodides, followed by addition of the tetraethyl methylenebis-(phosphonate) anion, resulted in ~40−50% yield of the desired products **18**, contaminated with small amounts (<10%) of the corresponding dialkylated bisphosphonate byproducts.

Efforts to introduce a fluorine atom at Cα of the bisphosphonates using the conditions previously reported by McKenna and co-workers were mostly unsuccessful in the preparation of this library.[14] However, conversion of **18** to **19** was achieved in good to excellent yield using *N*-fluoro-*N*-(phenylsulfonyl) benzenesulfonamide (NFSI) as the fluorinating agent under strongly basic conditions; in general, NaH/15-Crown-5 or *n*-BuLi could be used to affect deprotonation at the Cα of the bisphosphonates with equivalent results (~80% yields). The subsequent Suzuki cross-coupling reactions of fragments **18** and **19** with various aryl and heteroaryl boronates (acids or esters), carried out under standard Pd-catalyzed conditions, produced the desired compounds with yields of 50−70%. *N*-Heterocyclic boronate reagents, particularly those bearing free amino moieties, are known to be challenging in Pd-catalyzed cross-coupling reactions, necessitating either the use of protecting groups on the nitrogen or specialized catalysts.[24,25] Indeed, higher yields were obtained when boronate fragments, such as the indazoles **f**, **w**, and **x** (Table 2), were protected with a tetrahydropyran (THP) group before used in the library synthesis. However, increasing the load of $Pd(PPh_3)_4$ catalysts to 20 mol % allowed us to avoid the use of protecting groups and obtain the desired products in reasonable yields and purity.

Table 2. Inhibition Data for Some Key Compounds[a]

compd	hFPPS final IC_{50} (nM)	compd	hFPPS final IC_{50} (nM)
1	4.1[b]	**13c**	150
2	11	**8f**	520
3	85	**13f**	430
8c	115	**13k**	28
9c	164	**13l**	35
11c	47	**13o**	35
12c	>10,000	**13v**	32

[a]Average IC_{50} values of three determinations; standard deviation of less than 10% was observed. [b]IC_{50} value reported by Kavanagh et al.[4]

Derivatives of general structures **13**−**16** were synthesized from the aminopyridine bromides. The 4-bromopyridin-2-amine was prepared from the 4-bromo-2-chloropyridine after activation of the aromatic ring to the 4-bromo-2-chloropyridine

Scheme 1. Parallel Synthesis of Inhibitors 8−16

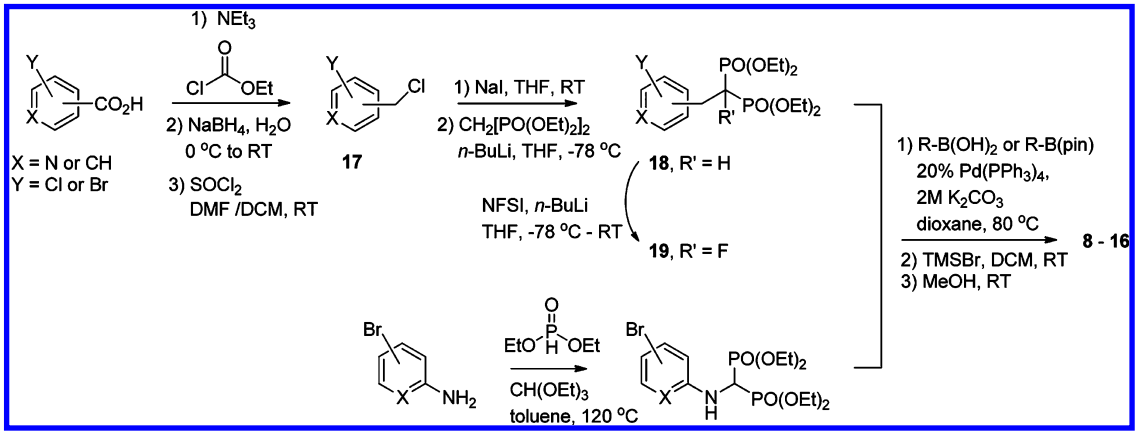

dx.doi.org/10.1021/jm201657x | J. Med. Chem. 2012, 55, 3201−3215

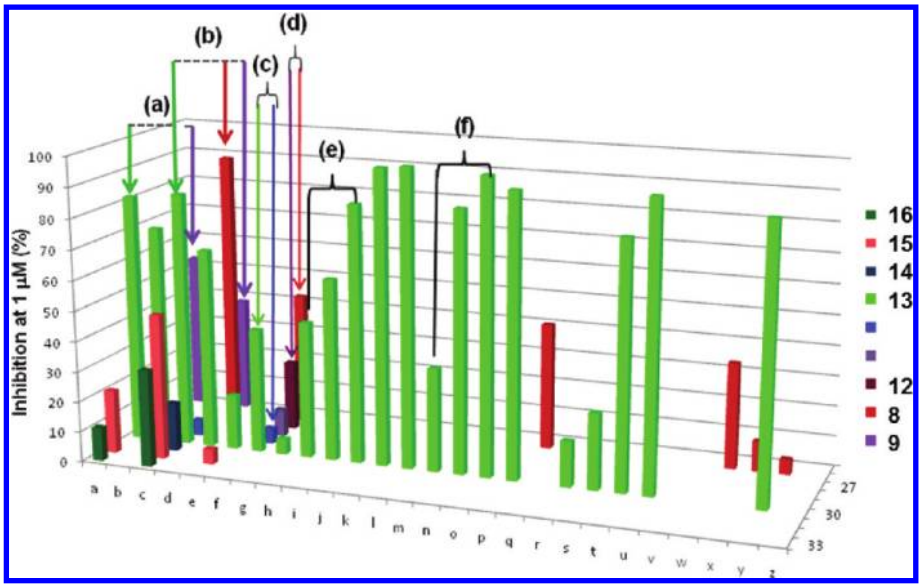

Figure 2. Inhibition of human FPPS at 1 μM concentration of each key compound from the permutation library shown in Table 1; average of three determinations (standard deviation of less than 10%).

1-oxide, displacement of the chloride with ammonia, and finally reduction with PBr_3 to give 4-bromopyridin-2-amine in modest overall yields (~20% over the three steps). Bromination of 2-animopyridine with *N*-BS provided the 5-bromopyridin-2-amine fragment. The 3-bromo- and 6-bromopyridin-2-amines are commercially available. These intermediates were subsequently reacted with diethylphosphite and triethyl orthoformate at high temperatures to obtain the corresponding tetraethyl bisphosphonate esters with yields ranging from 70 to 85%. Subsequent Suzuki cross-coupling reactions with a variety of boronates (acids or esters; Table 1), catalyzed by $Pd(PPh_3)_4$ under basic conditions, provided the desired bisphosphonate esters in isolated yields ranging from 40 to 85%.

During optimization of our synthetic methodologies, both the tetraisopropyl and the tetraethyl bisphosphonate esters were investigated. We found that both protecting groups provide advantages and disadvantages in the overall efficiency of a library synthesis and the isolation of the final compounds. Hydrolysis of the tetraisopropyl bisphosphonate esters in 6 N HCl, followed by precipitation of the products by the addition of DCM and MeOH, leads to the isolation of the corresponding phosphonic acids in low yields. The tetraethyl bisphosphonate esters were treated with TMSBr (to exchanges the ethyl esters with the trimethylsilyl esters) and subsequently treated with MeOH to obtain the final inhibitors as the phosphonic acids (isolated yields of 50−95%). Although acid hydrolysis of the tetraisopropyl bisphosphonate esters requires harsh conditions, it has the advantage of been reasonably fast (10−15 h), as compared to the hydrolysis of the tetraethyl bisphosphonate esters using TMSBr, which requires several days for complete conversion (3−5 days). In addition, we found that the quality of commercial TMSBr is highly variable (leading to reaction times that could exceed a 3 day period); thus, the progress of the reaction had to be followed by ^{13}P NMR to ensure complete conversion. All final products were isolated as white to pale yellow solids (precipitated out of solution with DCM/MeOH/H_2O). The final products were converted to the mono or disodium salts (by the addition of the required mole equivalents of NaOH) and used in the biological assays. Analogues **11** and **12** were synthesized from corresponding anilines using procedures similar to those outlined above (Scheme 1).

BIOLOGY

The main objective of this study was to identify low nanomolar lead compounds, rather than to fully investigate the SAR of all the analogues synthesized (Table 1). Consequently, all members of our library were initially screened in our hFPPS inhibition assay at a fixed concentration of 1 μM using compound **2** as the positive control.[23] The inhibition data observed for some of the most important analogues is summarized in Figure 2 (% inhibition of hFPPS at 1 μM of compound; average values of three determinations; standard deviation of less than 10% was observed). Full dose−response inhibition curves (IC_{50}) were subsequently determined for analogues exhibiting >80% inhibition at 1 μM concentration. *In vitro* data of key compounds are shown in Table 2. Consistent with previous SAR studies, replacement of the pyridine core with a phenyl ring, resulted in a dramatic loss of potency [e.g., **8f** vs **12f**; Figure 2d and **8c** vs **12c**; Table 2].[14,15] In general, the 2-aminopyridine derivatives **13** were almost equipotent to the Cα-fluoro pyridines **8**, whereas the Cα-deoxy analogues **9** were slightly less potent [e.g., Figure 2a and b]. Although no evidence of chemical instability was observed with any of the compounds in this library, due to some concerns about the chemical stability of Cα-fluoro bisphosphonates (**8**), we decided to focus our attention on the 2-aminopyridine series of compounds **13**−**16**.

Aminopyridine analogues **13** having a lipophilic moiety at -R_4 (e.g., derivatives **13a**, **13b**, and **13c**) were found to be more potent than those with polar moieties (e.g., derivatives **13e**, **13f**, and **13g**). Substitution at -R_3 was generally unfavorable; for example, an inhibitor having a phenyl group at -R_3 (e.g., **14c**) was found to be significantly less potent than the -R_4 analogue **13c** (16% inhibition vs 85% inhibition of hFPPS at 1 μM). This is in contrast to previously reported SAR where the 3-methylpyridin-2-amine derivative of compound **3** was found to be 2-fold more potent than **3**.[15] The $C_{pyridyl}$−N_{amino} bond has a partial double-bond character (mean length 1.35 Å) due to the

dx.doi.org/10.1021/jm201657x | *J. Med. Chem.* 2012, 55, 3201−3215

delocalization of the amino lone pairs into the pyridyl ring.[26] In solution, these compounds exist in dynamic equilibrium between the *E* and the *Z* isomer and the *E*/*Z* ratio is highly dependent on the substitution pattern of the pyridine ring.[26] The large -R_3 substituents of analogues **14** appear to disrupt the bioactive conformation of these compounds, leading to loss of potency.

The -R_5 (**15c**) and -R_6 (**16c**) derivatives were also less potent than the corresponding -R_4 derivatives (**13c**; Figure 2). Substitution around the -R_4 phenyl of analogue **13c** resulted in a sequential increase of potency as we moved the same substituent from the *ortho*, to *meta*, to *para* position. For example, the relative inhibition observed with the methoxy analogues **13h**, **13i**, and **13j** (at 1 μM) were 45%, 60%, and 85%, respectively [Figure 2e]. Similar results were observed with the methyl (**13m**, **13n**, and **13o**; Figure 2f] and other derivatives, providing some insight as to the available volume/space around these molecules when bound to the hFPPS active site. In summary, *para*-substitution of the -R_4 phenyl ring resulted in a substantial improvement in potency from our initial hits (~20-fold)[23] and provided the best analogues in this series (e.g., **13k**,**l**,**v**).

RESULTS AND DISCUSSION

The active site of hFPPS consists of a large partly lipophilic cavity, having two charged surfaces on opposite walls (Figure 3). One of these surfaces is composed of two conserved aspartate-rich motifs (^{117}DDIMD^{121} and ^{257}DDYLD^{261}) that bind the pyrophosphate moiety of the substrates DMAPP/GPP, or the bisphosphonate moiety of an *N*-BP inhibitor, via metal-mediated interactions. Adjacent to this surface is a lipophilic region, defined by the "capping" phenyls of Phe112 and Phe113, which control the polymerization of prenyl monomers to a C-15 chain (i.e., FPP).[27] The IPP binding subpocket is at the opposite wall of the cavity and lined with Arg and Lys residues that interact with its pyrophosphate (Figure 3). Co-crystal structures of clinically relevant *N*-BPs in complex with hFPPS have revealed that they bind exclusively to a small portion of the GPP subpocket through metal chelation of the bisphosphonate with 3Mg^{2+} ions.[3,4] Additionally, their nitrogen-containing side chains are in the protonated state and form bifurcated H-bond interactions with the carbonyl of Lys-200 and the hydroxyl of Thr-201 (Figure 3). It has been proposed that these interactions mimic the putative allylic carbocation transition-state during catalysis.[28] The Cα-hydroxyl moiety of *N*-BPs is also involved in interactions with the protein and maximizes the affinity of these drugs for bone minerals.[3,14]

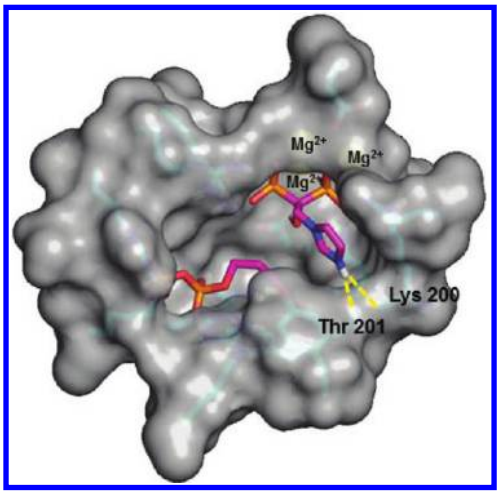

Figure 3. Active site cavity of the hFPPS/**1**/IPP ternary complex (PDB ID 1ZW5);[3] IPP and compound **1** are highlighted in magenta. Hydrogen-bond interactions are indicated with dashed yellow lines.

Large time-dependent shifts in potency have been reported for potent *N*-BP inhibitors of hFPPS, such as **1** and **2**,[3,4,15] and shown to correlate with tight binding of these inhibitors to the GPP subpocket of the enzyme, followed by binding of IPP and the subsequent induction of a conformational change that locks the active site cavity to a closed state.[3] Up to now, this nearly irreversible conformational change has been presumed to require the cobinding of IPP and has been proposed to be a strong indicator of the *in vivo* efficacy of potent *N*-BP drugs.[29] Under our assay conditions, the shift in IC_{50} of compound **2** was identical to that previously reported;[15] a ratio of 78-fold was observed for *initial* IC_{50}/*final* IC_{50}, determined without preincubation and with a 10 min preincubation of the enzyme with the inhibitor, respectively. In contrast, the IC_{50} shift observed for analogue **3** (the parent compound of our new hFPPS inhibitors) was minor (4.7-fold), suggesting that protein isomerization of the hFPPS/**3** complex was highly reversible. Significantly larger time-dependent shifts in IC_{50} were observed with analogues **13k** and **13l** (50- and 60-fold, respectively), consistent with the formation of stable hFPPS complexes. It is noteworthy that the time-dependent shifts in potency for inhibitors **13k** or **13l** are significantly greater than one would anticipate based on their potency as compared to that of the patent molecule **3** (Table 2). In an effort to explain this observation, we are currently exploring the 2-step mechanism of ligand binding, followed by conformational changes of the protein, which stabilize the closed conformation of the active site (i.e., the process responsible for the time-dependent shift in potency) in the presence and absence of IPP. The crystal structure of inhibitor **13k** bound to the active site of hFPPS (PDB ID 4DEM) provides some insight into this mechanism, pertaining specifically to this series of *N*-BP inhibitors.

Docking of compounds such as **13k**, **13l**, and **13v** (using GLIDE) to the fully closed active site of hFPPS (PDB ID 1ZW5) suggested that the larger side chain would forbid binding in the GPP subpocket alone without imposing a significant conformational rearrangement to the protein structure. Indeed, the cocrystal structure of hFPPS and analogue **13k** (Figure 4; PDB ID 4DEM) revealed that the inhibitor binds far deeper into the GPP subpocket than the side chains of **1** or **2**, displacing the capping phenyls (Phe 112/113) and Gln 185. This conformational change allows the 4-isopropoxyphenyl moiety of **13k** to insert between Phe 113 and the side-chain amide of Gln 185 and to engage in stacking interactions with these residues (Figure 4a). The side chain of **13k** is further stabilized by water-mediated H-bonding between the pyridine ring nitrogen and Gln 254. In addition, previous crystallographic studies have shown that the fully closed form involves substantial movement and folding of the C-terminal tail of hFPPS over the enzyme-bound IPP substrate; the C-terminal basic residues (^{364}KRRK^{367}) are essential for catalysis.[30] Interestingly, the hFPPS/**13k** complex adopts a closed conformation, similar to that observed in the hFPPS/IPP/**1** ternary complex, with the ^{364}KRRK^{367} tail folded over the IPP subpocket entry site (Figure 4b). To the best of our knowledge, this is the first example of such a conformational

dx.doi.org/10.1021/jm201657x | J. Med. Chem. 2012, 55, 3201−3215

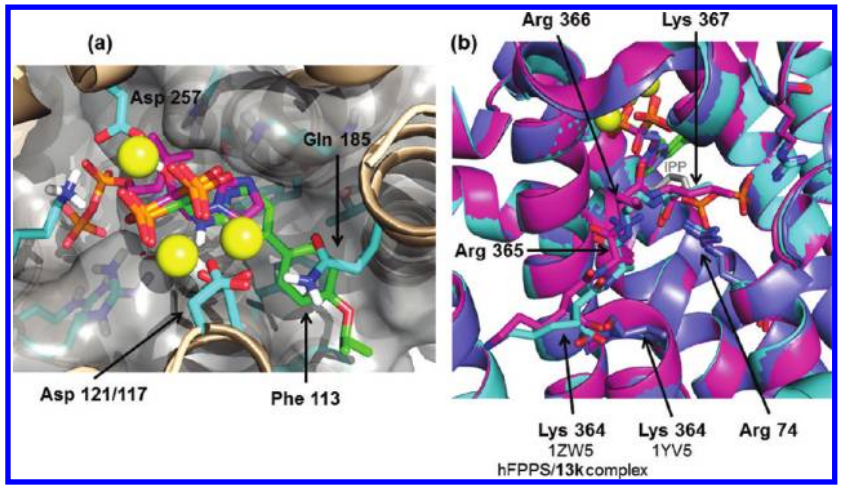

Figure 4. Superimposed X-ray structures of *N*-BPs and IPP bound to the active site of hFPPS. The IPP substrate and the bound inhibitors are shown in stick form. The carbon backbones of IPP and inhibitor **1** are highlighted in magenta, inhibitor **2** in blue, and inhibitor **13k** in green. Oxygen, nitrogen, and phosphorus atoms are colored in red, blue, and orange, respectively. The yellow spheres represent the Mg^{2+} ions. Key residues are indicated. (a) The surface of the active site is rendered semitransparent with residues covering the site removed for clarity. Superimposed ternary structure of hFPPS/IPP/**1** (PDB ID 1ZW5) and **13k** bound to hFPPS (PDB ID 4DEM). (b) Superimposed structures 1ZW5,[3] 1YV5,[4] and the hFPPS/**13k**-complex are shown in magenta, blue, and cyan, respectively. The ^{364}KRRK^{367} tail and the Arg 74 residue are shown in stick representation. The ^{364}KRRK^{367} tail is rigidified in the hFPPS/**13k** complex and the hFPPS/IPP/**1** ternary complex (1ZW5), but not in the hFPPS/**2** complex (1YV5); in the latter structure, Lys 364 of the KRRK tail is in a different conformation. Overall superimposition of the three structures (core rmsd: 0.32−0.44).

Table 3. Biological Profiling for Key Compounds

				predicted[b]		MM cells[c] EC_{50} (μM)		
compd	hFPPS initial IC_{50}[a] (nM)	hFPP final IC_{50}[a] (nM)	hGGPPS final IC_{50}[a] (nM)	SASA	FOSA	JJN3	RPMI-8226	KMS 28PE
1	475[d]	4.1[d]	IN	400	23	9.4	10.5	6.4
2	860	11	IN	410	24	10.0		10.6
13k	1,390	28	IN	580	110			
13l	2,090	35	IN	630	180			
13v	785	32	IN	680	220	8.6	3.6	3.2
4[e]	ND	100[e]	280[e]	ND	ND			
5	ND	>10,000	410	790	540			

[a]Initial and final IC_{50} values were determined without preincubation and with 10 min of preincubation, respectively; the average value of $n \geq 3$ determinations; standard deviation of ±5−10%. [b]Calculated using QikProp 3.2; total solvent accessible surface area in Å^2 using a probe with a 1.4 Å radius (SASA) and hydrophobic component (FOSA). IN = inactive (IC_{50} >100 μM). ND = not determined. [c]The average of $n \geq 8$ determinations; R^2 values in the range of 0.97−0.98. [d]IC_{50} value from Kavanagh et al.[4]. [e]IC_{50} value from Zhang et al.[19]. [f]ND = not determined.

change in the absence of bound IPP. A water-mediated hydrogen bond between the carbonyl of Arg 366 and the NH of the Asp 265 amide appears to contribute to holding the tail in the closed conformation. Other minor long-range conformational changes, induced by the binding of inhibitor **13k**, cannot be excluded. The IPP pocket is occupied by water molecules, and the volume of the H_2O-filled space can accommodate binding of IPP. We also observed that although the main chain of the ^{364}KRRK^{367} tail is rigidified in the hFPPS/**13k** complex, the side chains of these residues (Arg 365 and Lys 367 in particular) are flexible unlike those in the hFPPS/IPP/**1** ternary complex (PDB ID 1ZW5). It is important to note that the side chain of Lys 71, which makes a direct contact with the bound IPP in the hFPPS/IPP/**1** complex, is also poorly ordered in the hFPPS/**13k** complex. These side chains line up around the IPP subpocket and occlude a good portion of its entry site when rigidified in the presence of a bound IPP molecule. The flexibility of these side chains, therefore, may allow diffusion of IPP into the active site, in the hFPPS/**13k** secondary complex. We are currently pursuing both cocrystallization experiments of hFPPS with **13k** in the presence of IPP and "soaking" of the hFPPS/**13k** complex with IPP in the hope of obtaining additional structural information. ^{1}H NMR line broadening studies indicated that analogues from this new series of *N*-BPs compete for binding with both **2** and IPP (data shown in Supporting Information);[23] the latter observations may reflect the weak affinity of IPP for the GPP subpocket, in the absence of a higher affinity ligand.[3]

In line with our objectives, the most potent hFPPS inhibitors identified from our library were also found to be selective for the intended target and did not inhibit the functionally related enzyme hGGPPS. Several of our analogues were tested in inhibition assays using human recombinant GGPPS and compound **5** as the positive control. However, inhibition was not observed with any of our best inhibitors even at a compound concentration of 100 μM (Table 3). This is in contrast to previously reported *N*-BPs, which were designed to have larger side chains and higher lipophilicity than the current drugs, such as analogues **4** and **5**. These larger molecules are either more selective for the larger active site of hGGPPS (e.g., **5**) or are nearly equipotent in inhibiting both enzymes (e.g., **4**; Table 3).[16,17,19−21] It is possible that target selectivity will not

lead to any clinical complications for this class of drugs (particularly if they are exclusively absorbed into bone tissue) since inhibition of hFPPS down-regulates all downstream enzymes in the mevalonate pathway (Figure 1). Nonetheless, rigid molecules that exhibit target selectivity are less likely to produce off-target toxicities than highly flexible molecules that bind to multiple targets.

Clinical evidence is rapidly accumulating which implicates *N*-BP inhibitors of hFPPS as antineoplastic and specifically antimyeloma therapeutic agents.[6] Thus, extensive evaluation of the antimyeloma properties of our compounds is currently in progress. Preliminary antiproliferation and cytotoxic effects were observed with inhibitor **13v** and compared to those of **1** and **2** using three human MM cell lines. Cell viability was determined by MTT staining, and reductions in cell growth were noted with all three compounds. However, the median effective concentrations for 50% growth inhibition (EC_{50}) were consistently lower for compound **13v** as compared to those of **1** and **2**. The EC_{50} values shown in Table 3 represent the average of $n \geq 8$ determinations with R^2 in the range of 0.97−0.98. The improved cell-based potency of **13v** (as compared to **1** and **2**) may be due to its predicted higher lipophilicity (Table 3). We also explored the mechanism of cytotoxicity by examining the ability of **13v** to induce apoptosis. KMS28PE cells were treated with vehicle (control) or inhibitor **13v** at concentrations of 1 μM or 100 μM and cultured for 48 h (Figure 5). Apoptosis was determined by Annexin V staining of

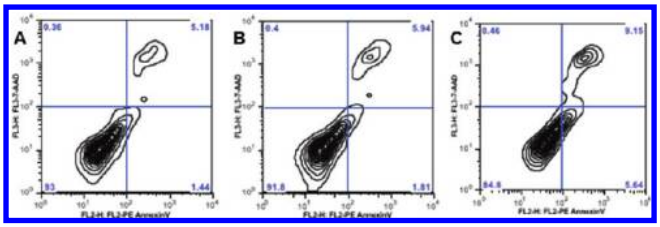

Figure 5. Flow cytometric evaluation of 7-AAD staining for cell viability analysis and detection of Annexin V-positive apoptotic multiple myeloma KMS28PE cells treated with either the vehicle alone (A) or 1 μM (B) or 100 μM (C) of compound **13v** for 48 h in culture.

KMS28PE cells and detected by flow cytometry, demonstrating a dose-responsive increase in the apoptotic fraction (Figure 5; 6.98% for controls vs 15.25% for 100 μM of **13v**). To further elucidate the mechanism of action, we investigated the ability of **13v** to inhibit phosphorylation of ERK (extracellular-signal regulated kinase 1/2, also known as p42/p44 mitogen activated protein-extracellular or MAPK), a signaling protein downstream from Ras (Figure 1). We noted a rapid reduction (most evident after 10 min) in the phosphorylated fraction of pERK following treatment of MM cells with **13v**, while total ERK levels did not change (Figure 6).

CONCLUSIONS

Herein we disclose the hit-to-lead optimization of a new series of *N*-BPs, enabling the identification of potent and selective inhibitors of hFPPS. The heterocyclic side chain of these inhibitors does not engage in hydrogen-bond interactions with Lys 200 and Thr 201. These hydrogen bonds are known to contribute significantly to the potency of the current *N*-BP drugs in inhibiting hFPPS (>280-fold loss in potency was reported by Dunford et al. when the pyridine side chain of **2**

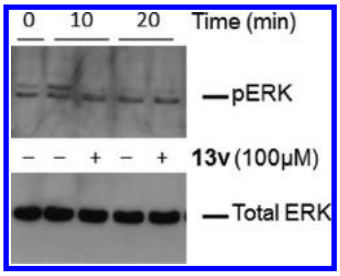

Figure 6. Effect of inhibitor **13v** on ERK signaling. Immunoblots showing total and phosphorylated ERK (pERK1,2 isoforms) expression in RPMI 8226 cells following FBS stimulation after overnight serum starvation at the times indicated with and without the addition of inhibitor **13v**.

was replaced by a phenyl).[15] The crystal structure of analogue **13k** bound to the active site reveals the induction of several conformational changes to residues within the GPP lipophilic subsite and a series of new interaction with the active site cavity. In addition, the C-terminal tail of hFPPS was shown to assume an unexpected rigidified conformation that was previously observed only in ternary complexes, thus revealing that cobinding of IPP is not an absolute requirement for induction of the active site closed conformation. Members of this series of *N*-BPs induce cytotoxicity and apoptosis in human multiple myeloma cell lines and down-regulate the intended intracellular target in these cells, as evidenced by the inhibition of a downstream phosphorylation event. Future studies will concentrate on enhancing our understanding of the inhibitor-induced hFPPS conformational changes and their impact on inhibition potency and selectivity for this target. Our current lead optimization efforts are focused on improving cell-based potency, an essential prerequisite in developing a therapeutic agent for treating multiple myeloma and possibly other nonskeletal cancers.

EXPERIMENTAL SECTION

General. All intermediate compounds were purified by normal phase flash column chromatography on silica gel using a CombiFlash instrument and the solvent gradient indicated. Library analogues were also purified at the bisphosphonate tetraester stage by normal-phase chromatography on silica gel (using a CombiFlash instrument). The purified bisphosphonate tetraesters were analyzed for homogeneity by reversed-phase HPLC and fully characterized by ^{1}H, ^{13}C, and ^{31}P NMR, and MS. The homogeneity of all bisphosphonate tetra esters (i.e., immediate precursors to the final inhibitors) was confirmed by C18 reversed phase HPLC, using either Method A or Method B indicated below; chromatograms of representative examples are shown in the Supporting Information. In general, the tetraester intermediates were purified to >90% homogeneity before proceeding to the final deprotection step and the isolation of the bisphosphonic acids (i.e., final inhibitors). After ester hydrolysis, the final bisphosphonic acid products were precipitated and washed with HPLC grade DCM, MeOH, and small amounts of deionized H_2O to obtain the inhibitors as white solids; quantitative conversion of each tetraester to the corresponding bisphosphonic acid was confirmed by ^{31}P NMR. All final products were characterized by ^{1}H, ^{13}C, ^{31}P, and ^{19}F NMR and HR-MS. Chemical shifts (δ) are reported in ppm relative to the internal deuterated solvent (^{1}H, ^{13}C) or external H_3PO_4. (δ 0.00 ^{31}P), unless indicated otherwise. Low- and high-resolution MS spectra were recorded at the McGill University, MS facilities using electrospray ionization ($ESI^{\pm}$). The homogeneity of the final inhibitors was confirmed by HPLC using Method C (indicated below). Only samples with >95% homogeneity were tested in the enzymatic assays for the determination of IC_{50} values; the chromatograms of representative examples are shown in the Supporting Information.

dx.doi.org/10.1021/jm201657x | *J. Med. Chem.* 2012, 55, 3201−3215

HPLC Analysis of Bisphosphonate Tetraethyl Esters. For Method A, an Agilent Technology instrument was used, equipped with an Eclipse XDB-C-18, 5 μm, 4.6 × 150 mm column. Solvent A: 95% H_2O, 5% CH_3CN, and 0.05% TFA. Solvent B: 50% H_2O, 50% CH_3CN, and 0.05% TFA. Mobile phase: 1 min at 100% A, gradient from A to B in 5 min, then 15 min at 100% B. Flow rate: 1 mL/min. For Method B, a Waters e2695 instrument was used, equipped with Waters C-18, 3.5 μm column. Solvent A: H_2O and 0.1% FA. Solvent B: CH_3CN and 0.1% TFA. Mobile phase: gradient from 95% A to 95% B in 13 min. Flow rate: 1 mL/min.

HPLC Analysis of Final Inhibitors. For Method C, a Waters ALLIANCE instrument was used, equipped with a Waters Xselect CSH fluoro-phenyl, 5 μm column. Solvent A: H_2O and 0.06% TFA. Solvent B: CH_3CN and 0.06% TFA. Mobile phase: gradient from 100% solvent A to 50% solvent A in 10 min, then 15 min at 100% B. Flow rate: 1 mL/min.

Library Synthesis. *Synthesis of Benzylic Chlorides **17**. (5-Bromopyridin-3-yl)methanol.* To a solution of 5-bromonicotinic acid (1.00 g; 4.95 mmol) in anhydrous THF (30 mL), Et_3N (0.76 mL; 5.44 mmol) was added via syringe, and the solution was flushed with Argon and cooled to 0 °C. Ethylchloroformate (0.52 mL; 5.44 mmol) was then added dropwise via syringe, and the reaction mixture was stirred at RT for 1 h. The reaction mixture was filtered, the precipitate washed with THF (2×, 5 mL), and the filtrate was transferred to a clean RBF and cooled to 0 °C. $NaBH_4$ (468 mg; 12.4 mmol) was added in small portions, followed by the dropwise addition of H_2O (5 mL). The reaction mixture was stirred at RT overnight and then concentrated under vacuum. The aqueous crude mixture was extracted with EtOAc (6×, 10 mL), the organic layers were combined, dried over anhydrous Na_2SO_4, concentrated under vacuum, and purified by normal phase column chromatography on silica gel (silica gel was prewashed with 1% NEt_3 in hexanes/EtOAc, 3:1 ratio) using a CombiFlash instrument and a solvent gradient from 100% hexanes to 100% EtOAc. The desired product, compound was isolated as a colorless oil (426 mg; 46% yield).

^{1}H NMR (300 MHz, $CDCl_3$) δ 8.60 (d, J = 2.2 Hz, 1H), 8.50 (s, 1H), 7.89 (s, 1H), 4.74 (d, J = 5.8 Hz, 2H), 1.96 (t, J = 5.7 Hz, 1H). ^{1}H NMR is consistent with literature data.[40]

*3-Bromo-5-(chloromethyl)pyridine (**17**).* To an ice cold solution of the above alcohol (1.00 g, 5.35 mmol) in anhydrous DCM (15 mL), thionyl chloride (0.43 mL, 5.88 mmol, 1.1 eq) was added via syringe, and the mixture was stirred at RT for 3 h. The reaction was quenched with saturated aqueous $NaHCO_3$ (∼10 mL), the product was extracted into DCM (3 × 25 mL), dried over anhydrous Na_2SO_4, and concentrated to dryness under vacuum to give the desired product **17** as a pale yellow solid (1.09 g) in nearly quantitative yield and sufficiently pure to be used directly in the next step without purification.

^{1}H NMR (400 MHz, $CDCl_3$) δ 8.64 (s, 1H), 8.54 (s, 1H), 7.90 (t, J = 2.1 Hz, 1H), 4.56 (s, 2H).

4-Bromopyridin-2-amine. To a solution of 4-bromo-2-chloropyridine (120 μL, 1.08 mmol) in DCM (10 mL), *m*-chloroperbenzoic acid (932 mg, 3.78 mmol) was added in portions. The mixture was stirred at 50 °C overnight. The solution was cooled to room temperature, diluted with EtOAc (75 mL), and washed by saturated aqueous sodium bisulfite (50 mL) and $NaHCO_3$ (50 mL). The organic layer was dried over anhydrous $MgSO_4$, concentrated, and purified by chromatography on silica gel, using a solvent gradient from 1% to 20% of EtOAc in hexanes, to give the *N*-oxide as a colorless oil (200 mg, 89%). ^{1}H NMR (300 MHz, $CDCl_3$) δ 8.17 (d, J = 5.4 Hz, 1H), 7.64 (d, J = 2.1 Hz, 1H), 7.32 (dd, J = 5.4, 2.1 Hz, 1H).

A solution of the *N*-oxide (20 mg, 0.096 mmol, in 1 mL of MeOH) was placed in a pressure vessel, excess ammonium hydroxide (∼40 equiv) was added, and the mixture was stirred at 100 °C overnight. The solution was cooled to RT, diluted with EtOAc, and extracted with brine. The organic layers were collected, dried over anhydrous $MgSO_4$, concentrated, and purified by chromatography on silica gel, using a solvent gradient of 0% to 20% MeOH in EtOAc, to give the 2-amino-4-bromopyridine 1-oxide as a white solid (12 mg, 66% yield). ^{1}H NMR (300 MHz, CD_3OD) δ 7.91 (dd, J = 7.1, 0.4 Hz, 1H), 7.11 (dd, J = 2.7, 0.4 Hz, 1H), 6.85 (dd, J = 7.1, 2.7 Hz, 1H).

Finally, the a solution of the above product (45 mg, 0.24 mmol) in DCM(1 mL) was cooled in an ice bath, and PBr_3 (224 μL, 2.38 mmol) was added dropwise. The reaction mixture was allowed to warm-up and stir at 50 °C overnight. The solution was cooled to RT and concentrated under vacuum. The residue was diluted in DCM and extracted with aqueous 1 M NaOH and brine. The organic layer was dried over anhydrous $MgSO_4$, concentrated, and purified by chromatography on silica gel (solvent gradient from 1% to 15% of EtOAc in hexanes) to give the 2-amino-4-bromopyridine as a white solid (11.6 mg, 28% yield). ^{1}H NMR (300 MHz, $CDCl_3$) δ 7.88 (d, J = 5.4 Hz, 1H), 6.79 (dd, J = 5.4, 1.5 Hz, 1H), 6.67 (d, J = 1.5 Hz, 1H).

*General Procedure for the Synthesis of the Tetraethyl Bisphosphonate Esters (**18**) from Chloride **17**.* To a solution of 3-bromo-5-(chloromethyl)pyridine (**17**, 1 equiv) in anhydrous THF, NaI (1.1 equiv) was added, and the suspension was stirred at 60 °C for 1.5 h to form the benzylic iodide. In a separate flask, to a cooled solution (−78 °C) of tetraethyl methylenebis(phosphonate) (1 equiv) in anhydrous THF, *n*-BuLi (1.1 equiv) was added dropwise under Argon. The mixture was stirred at 0 °C for 5 min and recooled to −78 °C. The benzylic iodide was then transferred to the solution of the tetraethyl methylenebis(phosphonate) anion via a cannula. The reaction mixture was stirred at −78 °C for 1 h and at RT for 13 h. Quenched with a drop of MeOH and concentrated under vacuum. The residue was dissolved in EtOAc and washed with H_2O, 0.3 M aqueous $Na_2S_2O_3$, and brine. The EtOAc solution was dried over anhydrous Na_2SO_4 and purified by normal phase flash column chromatography on silica gel (silica was prewashed with 0.1% NEt_3 in hexanes/EtOAc, 3:1 ratio) using a CombiFlash instrument and a solvent gradient from 1% EtOAc in hexanes to 100% EtOAc and then to 10% MeOH in EtOAc. The isolated product was contaminated with some of the tetraethyl methylenebis(phosphonate) reagent. This mixture was redissolved in excess toluene, washed with H_2O (5×) and brine, dried over anhydrous Na_2SO_4, and concentrated under vacuum to give the desired compound **18** as a clear oil, in 40−50% yield and 87% purity (estimated by ^{13}P NMR). The impurity was determined to be the dialkylated byproduct, which was eliminated after the subsequent step.

^{1}H NMR (400 MHz, $CDCl_3$) δ 8.54 (s, 1H), 8.44 (s, 1H), 7.79 (s, 1H), 4.25−4.01 (m, 8H), 3.23 (td, J = 16.2, 6.4 Hz, 2H), 2.55 (tt, J = 23.7, 6.4 Hz, 1H), 1.39−1.24 (m, 11H).

^{31}P NMR (81 MHz, $CDCl_3$) δ 23.05.

^{13}C NMR (75 MHz, $CDCl_3$) δ 150.36, 148.93, 148.57, 141.53, 139.22, 62.79 (dd, J = 17.7, 6.9 Hz), 38.78 (t, J = 133.5 Hz), 28.40 (t, J = 4.8 Hz), 17.09−14.20 (m).

MS (ESI^+): calcd 480.03, 482.03 ($C_{15}H_{26}BrNNaO_6P_2$); found (m/z) 480.0 and 482.0 $[M + Na^+]^+$.

General Procedure for the Synthesis of the 2-Aminopyridinyl Tetraethyl Bisphosphonate Esters. In a pressure vessel, the 2-aminopyridyl bromides (1 equiv), triethyl orthoformate (6 equiv), and diethylphosphite (1.2 equiv) were dissolved in toluene and stirred at 130 °C for 3 days. The solution was cooled to room temperature, and the solvent was removed under vacuum. The residue was purified by silica gel chromatography on a CombiFlash instrument, using a solvent gradient from 1:1 EtOAc/hexanes to 100% EtOAc and then to 20% MeOH in EtOAc to give the tetraethyl bisphosphonate esters in 70−85% isolated yield.

Replacement of 2-aminopyridylbromides with 3-bromoaniline in the above protocol led to the preparation of the corresponding tetraethyl bisphosphonate ester intermediates used in the synthesis of final compounds **12**.

General Procedure for Fluorination at Cα to the Bisphosphonate Ester. A solution of the bisphosphonate tetraester (**18**; 1 equiv) in anhydrous THF was cooled to −78 °C, and *n*-BuLi (1.6 M in Hex, 1.1 equiv) was added via syringe. The solution was stirred for 10 min at −78 °C, allowed to warm-up to 0 °C, and stirred for 1 h, and then cooled back to −78 °C. After 10 min at −78 °C, a cold solution of *N*-fluoro-*N*-(phenylsulfonyl)benzenesulfonamide (1.12 equiv at 0 °C) in

anhydrous THF was added dropwise via syringe. The reaction mixture was stirred at −78 °C for 10 min and left to warm-up to RT and stirred overnight. The reaction mixture was quenched with the addition of saturated aqueous NH_4Cl, concentrated under vacuum, redissolved in EtOAc, and washed with water (3×) and brine. The organic layer was dried over anhydrous $MgSO_4$, concentrated to dryness under vacuum, and purified by normal phase column chromatography on silica gel using a CombiFlash instrument and a solvent gradient from 1:1 EtOAc/hexanes to 100% EtOAc and then to 10% MeOH in EtOAc. The fluorinated intermediate (e.g., compound **19**) was isolated as a clear to pale brown yellow oil in 60−75% yields (based on the recovery of some unreacted starting material).

General Procedure for Suzuki Cross-Coupling. A suspension of the pyridyl bromides (1 equiv), $Pd(PPh)_4$ (0.2 equiv), and boronic acid or boronate ester (1.5 equiv) in dimethoxyethane was degassed and then flashed with Argon. A solution of 2 M K_2CO_3 (2.5 equiv) was added, and the mixture was flushed again with Argon. The reaction mixture was stirred at 80 °C for 15 h. The solution was filtered through Celite, and the Celite was rinsed with 5% MeOH in EtOAc (3×). The eluents were concentrated and the residue was purified by silica gel chromatography using a CombiFlash instrument and a solvent gradient from 1:1 EtOAc/hexanes to 100% EtOAc and then to 20% MeOH in EtOAc; isolated yields of the desired product varied from 45%−95%.

General Procedure for the Hydrolysis of the Tetraethyl Bisphosphonate Esters. A solution of the tetraethyl bisphosphonate ester (1 equiv) in CH_2Cl_2 was cooled to 0 °C, and trimethylsilyl bromide (15 equiv) was added. The reaction mixture was stirred at room temperature for 2 days (longer reaction periods of up to 5 days were required when the TMSBr reagent was old); the completion of conversion was monitored by ^{31}P NMR. The mixture was then diluted with HPLC grade MeOH (∼10 mL) and stirred at RT for 1 h, the solvent was evaporated to dryness, and this step was repeated four times. The organic solvents were evaporated under vacuum, the residue was dissolved in 0.5 mL of MeOH, and excess CH_2Cl_2 (∼10 mL) was added to induce precipitations of the final product. In cases where the final solid was colored or more like a gum than a solid, the sample was redissolved in HPLC-grade MeOH, the flask was placed in a sonicating bath for a few minutes to ensure particle dispersion, and the desired product was precipitated out of solution by the addition of deionized water. The amorphous powder was collected by filtration, washed with DCM (2×) and Et_2O (2×), and dried under vacuum to give the final compound as a white solid in nearly quantitative yields.

Key Examples of Compound Characterization: NMR and MS Data. *Inhibitor* ***3***. ^1H NMR (200 MHz, D_2O) d 7.67 (d, J = 4.2 Hz, 1H), 7.30 (dd, J = 7.8, 7.8 Hz, 1H), 6.31−6.44 (m, 2H), 3.61 (dd, J = 19.4, 19.4 Hz, 1H).

^{13}C NMR (125 MHz, D_2O) δ 156.67, 142.78, 139.65, 112.22, 109.84, 51.59 (CH, t, J = 122.4 Hz); ^{31}P NMR (D_2O) d 15.22. MS calcd for $C_6H_9N_2O_6P_2$ m/z 266.9941 $(M - H^+)^-$; found m/z 267.05

Inhibitor ***8c***. ^1H NMR (500 MHz, D_2O) δ 8.51 (d, J = 2.2 Hz, 1H), 8.41 (s, 1H), 8.06 (s, 1H), 7.66 (d, J = 7.2 Hz, 1H), 7.45 (t, J = 7.6 Hz, 2H), 7.36 (t, J = 7.4 Hz, 1H), 3.51−3.33 (m, 2H).

^{13}C NMR (75 MHz, D_2O) δ 149.46, 144.16, 138.18, 137.45, 135.40, 129.10, 128.09, 127.10, 35.40. ^{19}F NMR (470 MHz, D_2O) δ −185.66 to −186.35 (m).

{^{19}F, ^{13}C}HMQC NMR (470 MHz, D_2O) δ −186 (^{19}F) correlates with 100 (^{13}C).

^{31}P NMR (81 MHz, D_2O) δ 13.01 (d, J = 66.2 Hz).

HRMS: calcd for $C_{13}H_{13}FNO_6P_2$ m/z 360.0208 $(M - H^+)^-$; found m/z 360.0219

Inhibitor ***8f***. ^1H NMR (500 MHz, D_2O) δ 8.34 (s, 1H), 8.24 (s, 1H), 7.95 (s, 1H), 7.94 (s, 1H), 7.81 (s, 1H), 7.47 (dd, J = 26.9, 8.7 Hz, 2H), 3.41−3.28 (m, 2H).

^{13}C NMR (126 MHz, D_2O) δ 149.01 (s), 143.57 (s), 142.80 (s), 138.17 (s), 135.60 (s), 135.02−134.83 (m), 134.42 (s), 129.36 (s), 125.40 (s), 123.16 (s), 118.91 (s), 112.30 (s), 99.63 (dt, J = 177.2, 136.0 Hz), 36.64 (d, J = 18.1 Hz).

{^{19}F, ^{13}C}HMQC NMR (470 MHz, D_2O) δ −185 (^{19}F) correlates with δ 99 (^{13}C).

^{31}P NMR (81 MHz, D_2O) δ 12.86 (d, J = 66.7 Hz).

^{19}F NMR (470 MHz, D_2O) δ −184.77−185.26 (m).

HRMS (ESI^-): calcd 400.02691 ($C_{14}H_{13}O_6N_3FP_2$); found (m/z) 400.02648 $(M - H^+)^-$.

Inhibitor ***9a***. ^1H NMR (500 MHz, D_2O) δ 8.50 (d, J = 2.1 Hz, 1H), 8.28 (d, J = 2.0 Hz, 1H), 8.02 (t, J = 2.1 Hz, 1H), 7.71−7.65 (m, 1H), 7.44 (s, 1H), 7.44 (d, J = 0.6 Hz, 1H), 3.03 (td, J = 15.2, 6.8 Hz, 3H), 2.05 (tt, J = 21.1, 6.8 Hz, 1H).

^{13}C NMR (126 MHz, D_2O) δ 147.49, 143.57, 138.53, 138.17, 135.16, 131.03, 127.31, 125.89, 122.04, 41.24 (t, J = 110.9 Hz), 28.86.

^{31}P NMR (81 MHz, D_2O) δ 18.66 (s).

HRMS: calcd for $C_{11}H_{12}NO_6P_2S$ m/z 347.9866 $(M - H^+)^-$; found m/z 347.9859.

Inhibitor ***9c***. ^1H NMR (500 MHz, D_2O) δ 8.47 (d, J = 2.1 Hz, 1H), 8.37 (d, J = 1.9 Hz, 1H), 8.02 (s, 1H), 7.63 (d, J = 7.2 Hz, 2H), 7.42 (t, J = 7.6 Hz, 2H), 7.34 (t, J = 7.4 Hz, 1H), 3.08 (td, J = 15.3, 7.0 Hz, 2H), 2.09 (tt, J = 21.0, 6.9 Hz, 1H).

^{13}C NMR (126 MHz, D_2O) δ 147.81, 144.19, 138.38, 137.34, 136.06, 135.99, 129.08, 128.14, 127.07, 41.23 (t, J = 110.6 Hz), 28.88.

^{31}P NMR (81 MHz, D_2O) δ 19.83 (s).

HRMS: calcd for $C_{13}H_{14}NO_6P_2$ m/z 342.0302 $(M - H^+)^-$; found m/z 342.0301.

Inhibitor ***11c***. ^1H NMR (500 MHz, D_2O) δ 8.05 (dd, J = 6.0, 2.2 Hz, 2H), 7.80−7.75 (m, 2H), 7.57 (t, J = 7.6 Hz, 2H), 7.52−7.47 (m, 1H), 7.46 (s, 1H), 3.80 (t, J = 19.0 Hz, 2H).

^{13}C NMR (75 MHz, D_2O) δ 137.83, 136.75, 134.14, 133.73, 133.53, 128.98, 128.06, 127.04, 117.68 (C-α triplet of the bisphosphonate moiety is not clearly visible; however, by HSQC $^1H-^{13}C$ correlation it was observed for ^1H at 3.80 ppm to ^{13}C at 52.25 ppm.

^{31}P NMR (81 MHz, D_2O) δ 14.97 (s); HRMS: calcd 343.0249 for (C12H13N2O6P2); found m/z 343.0251 $[M - H]^-$.

Inhibitor ***12c***. ^1H NMR (500 MHz, D_2O) δ 7.59 (d, J = 7.4 Hz, 1H), 7.38 (t, J = 7.7 Hz, 1H), 7.28 (t, J = 7.4 Hz, 1H), 7.19 (t, J = 7.9 Hz, 1H), 6.97 (s, 1H), 6.84 (d, J = 7.6 Hz, 1H), 6.71 (dd, J = 8.2, 2.1 Hz, 1H), 3.69 (t, J = 18.9 Hz, 1H).

^{13}C NMR (125 MHz, $CDCl_3$) δ 161.28, 149.28, 141.50, 140.85, 129.93, 128.94, 127.58, 126.90, 115.12, 112.32, 111.58, 52.48 (CH, t, J = 123.9 Hz).

^{31}P NMR ($CDCl_3$) δ 16.57.

HRMS: calcd for $C_{13}H_{14}NO_6P_2$ m/z 342.0302 $(M - H^+)^-$; found m/z 342.03043.

Inhibitor ***12f***. ^1H NMR (300 MHz, D_2O) δ 8.00 (s, 1H), 7.90 (s, 1H), 7.56 (d, J = 8.7 Hz, 1H), 7.49 (d, J = 8.7 Hz, 1H), 7.12 (dd, J = 7.8, 7.8 Hz, 1H), 6.85 (s, 1H), 6.70 (d, J = 7.8 Hz, 1H), 6.56 (d, J = 7.8 Hz, 1H), 3.52 (t, J = 19.5 Hz, 1H).

^{13}C NMR (75 MHz, D_2O) δ 149.92 (C), 141.72 (CH), 140.89 (C), 134.47 (C), 133.83 (C), 129.81 (CH), 126.53 (CH), 123.04 (C), 118.52 (CH), 113.58 (CH), 111.26 (CH), 111.03 (CH), 53.61 (CH).

^{31}P NMR (81 MHz, D_2O) δ 17.46.

HRMS: calcd for $C_{14}H_{14}N_3O_6P_2$ m/z 382.0363 $(M - H^+)^-$. found m/z 382.0374.

Inhibitor ***13a***. ^1H NMR (300 MHz, D_2O) δ 7.77 (dd, J = 3.0, 1.5 Hz, 1H), 7.71 (d, J = 6.0 Hz, 1H), 7.37−7.42 (m, 2H), 6.87 (s, 1H), 6.78 (d, J = 6.0 Hz, 1H), 3.85 (t, J = 21.0 Hz, 1H).

^{13}C NMR (75 MHz, D_2O) δ 157.77, 145.04, 144.33, 138.89, 127.31, 125.77, 124.34, 110.15, 105.56, 51.64 (CH, d, J = 121.5 Hz).

^{31}P NMR (81 MHz, D_2O) δ 15.07.

HRMS: calcd for $C_{10}H_{13}N_2O_6P_2S$ m/z 350.9964 $(M + H^+)^+$; found m/z 350.9955.

Inhibitor ***13b***. ^1H NMR (300 MHz, D_2O) δ 7.69 (d, J = 5.4 Hz, 1H), 7.48 (d, J = 3.0 Hz, 1H), 7.38 (d, J = 4.5 Hz, 1H), 6.99−7.03 (m, 1H), 6.83 (s, 1H), 6.74 (d, J = 4.5 Hz, 1H), 3.86 (t, J = 18.9 Hz, 1H).

^{13}C NMR (75 MHz, D_2O) δ 157.80 (C), 144.83 (C), 143.63 (CH), 140.68 (CH), 128.48 (CH), 127.87 (CH), 126.21 (CH), 109.42 (CH), 140.40 (C), 51.34 (CH, t, J = 116.0 Hz).

^{31}P NMR (81 MHz, D_2O) δ 15.12.

HRMS: calcd for $C_{10}H_{13}N_2O_6P_2S$ m/z 350.9964 $(M + H^+)^+$; found m/z 350.9957.

Inhibitor ***13c***. ^{1}H NMR (300 MHz, D_2O) δ 7.77 (d, J = 5.6 Hz, 1H), 7.62 (dd, J = 8.4, 1.8 Hz, 1H), 7.28−7.39 (m, 3H), 6.71 (s, 1H), 6.66 (d, J = 5.6 Hz, 1H), 3.79 (t, J = 21.3 Hz, 1H).
^{13}C NMR (75 MHz, D_2O) δ 161.79, 152.30, 149.69, 141.02, 131.50, 129.44, 112.32, 107.76, 54.71 (CH, J = 114.0 Hz).
^{31}P NMR (81 MHz, D_2O) δ 16.52.
HRMS: calcd for $C_{12}H_{15}N_2O_6P_2$ m/z 345.0400 $(M + H^+)^+$; found m/z 345.0393.
Inhibitor ***13d***. ^{1}H NMR (300 MHz, D_2O) δ 8.20 (s, 1H), 7.79−7.91 (m, 5H), 7.45−7.47 (m, 2H), 6.95 (s, 1H), 6.87 (d, J = 5.7 Hz, 1H), 3.92 (t, J = 19.3 Hz, 1H).
^{13}C NMR (75 MHz, D_2O) δ 158.93, 149.86, 146.64, 135.68, 133.08, 133.05, 128.55, 128.36, 127.55, 126.87, 126.72, 126.14, 124.75, 110.36, 105.79, 51.99 (CH, t, J = 125.0 Hz).
^{31}P NMR (81 MHz, D_2O) δ 15.56.
HRMS: calcd for $C_{16}H_{15}N_2O_6P_2$ m/z 393.0411 $(M - H^+)^-$; found m/z 393.0416.
Inhibitor ***13e***. ^{1}H NMR (500 MHz, D_2O) δ 8.73 (s, 1H), 8.43 (d, J = 5.1 Hz, 1H), 8.06 (d, J = 8.0 Hz, 1H), 7.88 (d, J = 5.5 Hz, 1H), 7.42 (dd, J = 8.0, 5.0 Hz, 1H), 6.85 (s, 1H), 6.77 (d, J = 5.1 Hz, 1H), 3.94 (t, J = 18.6 Hz, 1H).
^{13}C NMR (125 MHz, D_2O) δ 158.71, 148.69, 146.84, 135.84, 134.52, 128.11, 124.30, 110.34, 106.07, 51.37 (CH, t, J = 130.0 Hz).
^{31}P NMR (81 MHz, D_2O) δ 15.48.
HRMS: calcd for $C_{11}H_{12}N_3O_6P_2$ m/z 344.0207 $(M - H^+)^-$; found m/z 344.0215.
Inhibitor ***13f***. ^{1}H NMR (300 MHz, D_2O) δ 8.06 (s, 1H), 8.01 (s, 1H), 7.74 (d, J = 5.7 Hz, 1H), 7.46−7.55 (m, 2H), 6.74 (s, 1H), 6.71 (d, J = 5.7 Hz, 1H), 3.77 (t, J = 18.0 Hz, 1H).
^{13}C NMR (75 MHz, D_2O) δ 161.79, 153.25, 149.91, 149.53, 137.23, 131.63, 126.14, 125.94, 121.64, 116.34, 112.45, 107.47, 54.63 (CH, t, J = 171.0 Hz).
^{31}P NM (81 MHz, D_2O) δ 16.70.
HRMS: calcd for $C_{13}H_{15}N_4O_6P_2$ m/z 385.0461 $(M + H^+)^+$; found m/z 385.0457.
Inhibitor ***13g***. ^{1}H NMR (300 MHz, D_2O) δ 8.01 (s, 1H), 7.70−7.77 (m, 2H), 7.43 (d, J = 8.7 Hz, 1H), 6.85 (s, 1H), 6.76 (d, J = 5.1 Hz, 1H), 3.82 (t, J = 19.2 Hz, 1H).
^{13}C NMR (75 MHz, D_2O) δ 162.45, 157.70, 151.23, 146.57, 144.32, 132.98, 122.62, 116.42, 114.61, 110.89, 106.62, 51.96 (CH, t, J = 121.50 Hz).
^{31}P NMR (81 MHz, D_2O) δ 15.14.
HRMS: calcd for $C_{12}H_{12}N_5O_6P_2$ m/z 384.0268 $(M - H^+)^-$; found m/z 384.0270.
Inhibitor ***13h***. ^{1}H NMR (300 MHz, D_2O) δ 7.71 (d, J = 5.7 Hz, 1H), 7.25−7.32 (m, 2H), 6.92−7.01 (m, 2H), 6.92 (s, 1H), 6.61 (d, J = 5.7 Hz, 1H), 3.86 (t, J = 18.0 Hz, 1H), 3.66 (s, 3H).
^{13}C NMR (75 MHz, D_2O) δ 161.49, 157.40, 155.73, 148.82, 143.70, 130.40, 130.14, 127.67, 121.34, 113.40, 111.99, 55.48, 51.51 (CH, t, J = 134.03 Hz).
^{31}P NMR (81 MHz, D_2O) δ 15.19.
HRMS: calcd for $C_{13}H_{15}N_2O_7P_2$ m/z 373.0360 $(M - H^+)^-$; found m/z 373.0367.
Inhibitor ***13i***. ^{1}H NMR (300 MHz, D_2O) δ 7.77 (d, J = 5.7 Hz, 1H), 7.29 (dd, J = 7.6, 7.6 Hz, 1H), 7.20 (d, J = 7.6 Hz, 1H), 7.15 (d, J = 1.5 Hz, 1H), 6.90 (dd, J = 7.6, 1.5 Hz, 1H), 6.81 (s, 1H), 6.73 (d, J = 5.7 Hz, 1H), 3.91 (t, J = 19.2 Hz, 1H), 3.71 (s, 3H).
^{13}C NMR (75 MHz, D_2O) δ 159.19, 158.02, 150.22, 145.17, 139.68, 130.21, 119.80, 114.91, 112.27, 110.83, 106.49, 55.32, 51.35 (CH, t, J = 122.3 Hz).
^{31}P NMR (81 MHz, D_2O) δ 15.28.
HRMS: calcd for $C_{13}H_{15}N_2O_7P_2$ m/z 373.0360 $(M - H^+)^-$; found m/z 373.0364.
Inhibitor ***13j***. ^{1}H NMR (300 MHz, D_2O) δ 7.71 (d, J = 6.2 Hz, 1H), 7.55−7.59 (m, 2H), 6.89−6.94 (m, 2H), 6.82 (s, 1H), 6.74 (d, J = 6.2 Hz, 1H), 3.85 (t, J = 18.9 Hz, 1H), 3.68 (s, 3H).
^{13}C NMR (75 MHz, D_2O) δ 159.90, 130.19, 128.35, 114.36, 110.35, 105.96, 55.27, 51.76 (CH, t, J = 121.3 Hz).
^{31}P NMR (81 MHz, D_2O) δ 14.91.
HRMS: calcd for $C_{13}H_{17}N_2O_7P_2$ m/z 375.0506 $(M + H^+)^+$; found m/z 375.0492.
Inhibitor ***13k***. ^{1}H NMR (300 MHz, D_2O) δ 7.76 (d, J = 5.7 Hz, 1H), 7.60 (d, J = 8.7 Hz, 2H), 6.95 (d, J = 8.7 Hz, 2H), 6.81 (s, 1H), 6.74 (d, J = 5.7 Hz, 1H), 3.88 (t, J = 19.5 Hz, 1H), 1.19 (d, J = 6.0 Hz, 6H).
^{13}C NMR (75 Hz, D_2O) δ 158.03, 157.81, 149.86, 144.92, 130.73, 128.40, 116.57, 110.23, 105.61, 71.55, 51.67 (CH, t, J = 126.11 Hz), 20.95.
^{31}P NMR (81 MHz, D_2O) δ 15.26.
HRMS: calcd for $C_{15}H_{21}N_2O_7P_2$ m/z 403.0819 $(M + H^+)^+$; found m/z 403.0812.
Inhibitor ***13l***. ^{1}H NMR (500 MHz, D_2O) δ 7.78 (d, J = 5.5 Hz, 1H), 7.61 (d, J = 8.8 Hz, 2H), 6.90 (d, J = 8.8 Hz, 2H), 6.84 (s, 1H), 6.77 (d, J = 5.5 Hz, 1H), 3.92 (t, J = 18.0 Hz, 1H), 2.33−2.37 (m, 2H), 1.95−2.03 (m, 2H), 1.69−1.72 (m, 1H), 1.55−1.61 (m, 1H).
^{13}C NMR (125 Hz, D_2O) δ 157.96, 157.57, 149.95, 144.76, 130.67, 128.44, 115.51, 110.35, 105.72, 72.10, 51.59 (CH, t, J = 123.8 Hz), 29.86, 12.45.
^{31}P NMR (81 MHz, D_2O) δ 15.19.
HRMS: calcd for $C_{16}H_{19}N_2O_7P_2$ m/z 413.0673 $(M - H^+)^-$; found m/z 413.0667.
Inhibitor ***13m***. ^{1}H NMR (300 MHz, D_2O) δ 7.75 (d, J = 5.7 Hz, 1H), 7.17−7.21 (m, 4H), 6.51 (s, 1H), 6.45 (d, J = 5.7 Hz, 1H), 3.87 (CH, t, J = 19.2 Hz, 1H), 2.13 (s, 3H).
^{13}C NMR (75 MHz, D_2O) δ 157.75, 151.92, 144.55, 139.41, 135.40, 130.42, 128.89, 128.38, 125.95, 113,26, 109.26, 51.38 (CH, t, J = 124.5 Hz), 19.22.
^{31}P NMR (81 MHz, D_2O) δ 15.35.
HRMS: calcd for $C_{13}H_{15}N_2O_6P_2$ m/z 357.0411 $(M - H^+)^-$; found m/z 357.0420.
Inhibitor ***13n***. ^{1}H NMR (300 MHz, D_2O) δ 7.77 (d, J = 5.9 Hz, 1H), 7.47 (s, 1H), 7.41 (d, J = 7.6 Hz, 1H), 7.26 (dd, J = 7.6, 7.6 Hz, 1H), 7.17 (d, J = 7.6 Hz, 1H), 6.84 (s, 1H), 6.76 (d, J = 5.9 Hz, 1H), 3.90 (t, J = 18.9 Hz, 1H), 2.24 (s, 3H).
^{13}C NMR (75 Hz, D_2O) δ 157.98, 150.74, 144.87, 139.22, 137.88, 129.93, 128.99, 127.47, 123.94, 110.84, 106.43, 51.39 (CH, t, J = 120.0 Hz), 20.31.
^{31}P NMR (81 MHz, D_2O) δ 15.22.
HRMS: calcd for $C_{13}H_{15}N_2O_6P_2$ m/z 357.0411 $(M - H^+)^-$; found m/z 347.0418.
Inhibitor ***13o***. ^{1}H NMR (300 MHz, D_2O) δ 7.80 (d, J = 5.7 Hz, 1H), 7.57 (d, J = 8.1 Hz, 2H), 7.24 (d, J = 8.1 Hz, 2H), 6.84 (s, 1H), 6.77 (d, J = 5.7 Hz, 1H), 3.92 (t, J = 19.5 Hz, 1H), 2.25 (s, 3H).
^{13}C NMR (75 Hz, D_2O) δ 158.29, 150.24, 145.50, 134.99, 129.62, 126.83, 110.46, 105.27, 51.50 (CH, t, J = 227.5 Hz), 20.18.
^{31}P NMR (81 MHz, D_2O) δ 15.39; HRMS:calcd for $C_{13}H_{15}N_2O_6P_2$ m/z 357.0411 $(M - H^+)^-$; found m/z 357.0402.
Inhibitor ***13p***. ^{1}H NMR (500 MHz, D_2O) δ 7.81 (d, J = 5.2 Hz, 1H), 7.61 (d, J = 8.3 Hz, 2H), 7.34 (d, J = 8.3 Hz, 2H), 6.87 (s, 1H), 6.80 (d, J = 5.2 Hz, 1H), 3.95 (t, J = 19.5 Hz, 1H), 2.86 (septet, J = 7.0 Hz, 1H), 1.13 (d, J = 6.9 Hz, 6H).
^{13}C NMR (125 Hz, D_2O) δ 158.21, 150.91, 150.26, 145.31, 135.45, 127.14, 127.02, 110.59, 105.86, 51.46 (CH, t, J = 131.4 Hz), 33.31, 23.04.
^{31}P NMR (81 MHz, D_2O) δ 15.32.
HRMS: calcd for $C_{15}H_{19}N_2O_6P_2$ m/z 385.0724 $(M - H^+)^-$; found m/z 385.0736.
Inhibitor ***13r***. ^{1}H NMR (300 MHz, D_2O) δ 8.14 (s, 2H), 7.96 (s, 1H), 7.84 (d, J = 5.6 Hz, 1H), 6.81 (s, 1H), 6.74 (d, J = 5.6 Hz, 1H), 3.88 (t. J = 21.9 Hz, 1H).
^{13}C NMR (75 MHz, D_2O) δ 147.06, 144.05 (C, q, J = 548.8 Hz), 131.16 (C, q, J = 33.0 Hz), 128.76, 127.57−127.70 (CH, m), 125.14, 122.55−122.65 (CH, m), 121.53, 110.31, 105.01, 51.38 (CH, t, J = 120.8 Hz).
^{31}P NMR (81 MHz, D_2O) δ 15.46.
HRMS: calcd for $C_{14}H_{11}F_6N_2O_6P_2$ m/z 479.0002 $(M - H^+)^-$; found m/z 479.0020.

Inhibitor **13s**. ^{1}H NMR (300 MHz, D_2O) δ 7.90 (s, 1H), 7.79−7.81 (m, 2H), 7.60 (d, J = 8.0 Hz, 1H), 7.49 (dd, J = 8.8, 8.0 Hz, 1H), 6.82 (s, 1H), 6.74 (d, J = 5.7 Hz, 1H), 3.89 (t, J = 19.8 Hz, 1H).
^{13}C NMR (75 MHz, D_2O) δ 146.22, 144.01 (C, q, J = 701.4 Hz), 130.56, 130.12, 129.48, 125.82, 125.52 (CH, q, J = 4.5 Hz), 123.74 (CH, q, J = 1.3 Hz), 122.20, 110.55, 106.11, 51.31 (CH, t, J = 119.9 Hz).
^{31}P NMR (81 MHz, D_2O) δ 15.41.
HRMS: calcd for $C_{13}H_{12}F_3N_2O_6P_2$ m/z 411.0128 $(M - H^+)^-$; found m/z 411.0141.

Inhibitor **13t**. ^{1}H NMR (500 MHz, D_2O) δ 7.87 (d, J = 5.5 Hz, 1H), 7.78 (d, J = 8.3 Hz, 2H), 7.70 (d, J = 8.3 Hz, 2H), 6.89 (s, 1H), 6.80 (d, J = 5.5 Hz, 1H), 3.98 (t, J = 18.5 Hz, 1H).
^{13}C NMR (125 Hz, D_2O) δ 158.53, 149.10, 146.35, 141.90, 130.02 (C, q, J = 31.8 Hz), 127.47, 125.75 (CH, q, J = 15.0 Hz), 124.12 (C, q, J = 269.9 Hz), 110.79, 106.51, 51.15 (CH, t, J = 124.1 Hz).
^{31}P NMR (81 MHz, D_2O) δ 15.45.
HRMS: calcd for $C_{13}H_{12}F_3N_2O_6P_2$ m/z 411.0128 $(M - H^+)^-$; found m/z 411.0125.

Inhibitor **13u**. ^{1}H NMR (300 MHz, D_2O) δ 7.81 (d, J = 5.7 Hz, 1H), 7.62−7.67 (m, 2H), 7.11 (dd, J = 9.0, 9.0 Hz, 2H), 6,84 (s, 1H), 6.77 (d, J = 5,7 Hz, 1H), 3.93 (t, J = 19.2 Hz, 1H).
^{13}C NMR (75 MHz, D_2O) δ 163.18 (C, d, J = 245.1 Hz), 158.13, 149.65, 145.37, 134.13, 128.9 (CH, d, J = 8.5 Hz), 115.69 (CH, d, J = 21.6 Hz), 110.70, 106.10, 51.37 (CH, t, J = 122.0 Hz).
^{31}P NMR (81 MHz, D_2O) δ 15.43.
HRMS: calcd for $C_{12}H_{12}FN_2O_6P_2$ m/z 361.0160 $(M - H^+)^-$; found m/z 361.0153.

Inhibitor **13v**. ^{1}H NMR (500 MHz, D_2O) δ 7.80 (d, J = 5.9 Hz, 1H), 7.63 (d, J = 8.8 Hz, 2H), 6.98 (d, J = 8.8 Hz, 2H), 6.86 (s, 1H), 6.79 (d, J = 5.9 Hz, 1H), 4.85 (m, 1H), 3.93 (t, J = 17.5 Hz, 1H), 1.81−1.93 (m, 2H), 1.57−1.74 (m, 3H), 1.51−1.54 (m, 2H).
^{13}C NMR (125 MHz, D_2O) δ 158.14, 149.94, 145.03, 130.48, 128.36, 120.15, 116.28, 110.34, 105.52, 80.86, 51.56 (CH, t, J = 120.0 Hz), 32.14, 23.41.
^{31}P NMR (81 MHz, D_2O) δ 15.25.
HRMS: calcd for $C_{17}H_{21}N_2O_7P_2$ m/z 427.0829 $(M - H^+)^-$; found m/z 427.08355.

Inhibitor **13y**. ^{1}H NMR (300 MHz, D_2O) δ 7.79 (d, J = 5.4 Hz, 1H), 7.58 (d, J = 8,6 Hz, 2H), 7.36 (d, J = 8.6 Hz, 2H), 6.81 (s, 1H), 6,73 (d, J = 5,4 Hz, 1H), 3.90 (t, J = 18.9 Hz, 1H).
^{13}C NMR (75 MHz, D_2O) δ 149.27, 145.89, 136.61, 134.48, 128.89, 128.38, 126.91, 110.46, 105.91, 51.32 (CH, t, J = 119.3 Hz).
^{31}P NMR (81 MHz, D_2O) δ 15.41.
HRMS: calcd for $C_{12}H_{12}ClN_2O_6P_2$ m/z 376.9865 $(M - H^+)^-$; found m/z 376.9876.

Inhibitor **13z**. ^{1}H NMR (500 MHz, D_2O) δ 7.82 (d, J = 4.8 Hz, 1H), 7.67 (d, J = 8.5 Hz, 2H), 7.34 (t, J = 8.0 Hz, 2H), 7.13 (t, J = 7.4 Hz, 1H), 7.03 (m, 4H), 6.86 (s, 1H), 6.78 (d, J = 4.8 Hz, 1H), 3.94 (t, J = 20.0 Hz, 1H).
^{13}C NMR (125 MHz, D_2O) δ 159.14, 158.63, 156.94, 150.29, 146.77, 133.97, 130.86, 129.38, 124.90, 120.00, 119.49, 111.10, 106.37.
^{31}P NMR (81 MHz, D_2O) δ 15.20.
MS: calcd for $C_{18}H_{17}N_2O_7P_2$ m/z 435.0516 $(M - H^+)^-$; found m/z 435.11.

Inhibitor **14c**. ^{1}H NMR (300 MHz, D_2O) δ 7.77 (dd, 1H, J = 5.6, 1.5 Hz, 1H), 7.38−7.45 (m, 4H), 7.29−7.33 (m, 2H), 6.59 (dd, J = 5.6, 5.6 Hz, 1H), 4.19 (t, J = 19.5 Hz, 1H).
^{13}C NMR (75 MHz, D_2O) δ 154.37, 143.07, 138.76, 136.51, 129.32, 128.97, 128.20, 123.98, 112.31, 50.76 (CH, t, J = 120.0 Hz).
^{31}P NMR (81 MHz, D_2O) δ 15.01.
HRMS: calcd for $C_{12}H_{13}N_2O_6P_2$ m/z 343.0254 $(M + Na^+)^+$; found m/z 343.0254.

Inhibitor **15a**. ^{1}H NMR (300 MHz, D_2O) δ 8.07 (s, 1H), 7.70 (d, J = 9.0 Hz, 1H), 7.35−7.37 (m, 2H), 7.27 (d, J = 5.4 Hz, 1H), 6.62 (d, J = 8.7 Hz, 1H), 3.88 (t, J = 19.2 Hz, 1H).
^{13}C NMR (75 Hz, D_2O) δ 156.83, 142.61, 138.40, 136.85, 127.12, 125.27, 120.50, 118.77, 108.80, 51.03 (CH, t, J = 132.3 Hz).
^{31}P NMR (81 MHz, D_2O) δ 15.38.
HRMS: calcd for $C_{10}H_{11}N_2O_6P_2S$ m/z 348.9819 $(M - H^+)^-$; found m/z 348.9825.

Inhibitor **15c**. ^{1}H NMR (300 MHz, D_2O) δ 8.04 (s, 1H), 7.69 (d, J = 8.7 Hz, 1H), 7.46 (d, J = 7.6 Hz, 2H), 7.31 (dd, J = 7.6, 7.6 Hz, 2H), 7.19 (dd, J = 7.6, 7.6 Hz, 1H), 6.62 (d, J = 8.7 Hz, 1H), 3.85 (t, J = 19.2 Hz, 1H).
^{13}C NMR (75 Hz, D_2O) δ 157.47, 143.83, 137.65, 137.05, 129.04, 126.80, 125.66, 124.55, 108.35, 51.29 (CH, t, J = 123.8 Hz).
^{31}P NMR (81 MHz, D_2O) δ 15.47.
HRMS: calcd for $C_{12}H_{13}N_2O_6P_2$ m/z 343.0254 $(M - H^+)^-$; found m/z 343.0255.

Inhibitor **15f**. ^{1}H NMR (300 MHz, D_2O) δ 7.91−7.93 (m, 2H), 7.69 (s, 1H), 7.56 (d, J = 9.00 Hz, 1H), 7.41 (s, 2H), 6.53 (d, J = 9.00 Hz, 1H), 3.84 (t, J = 19.5 Hz, 1H).
^{13}C NMR (75 Hz, D_2O) δ 157.03, 143.45, 139.03, 137.09, 134.11, 130.62, 125.94, 124.70, 123.00, 117.12, 110.95, 108.15, 51.52 (CH, t, J = 120 Hz).
^{31}P NMR (81 MHz, D_2O) δ 15.23.
HRMS: calcd for $C_{13}H_{13}N_4O_6P_2$ m/z 383.0316 $(M - H^+)^-$; found m/z 383.0321.

Inhibitor **16a**. ^{1}H NMR (300 MHz, D_2O) δ 7.76 (d, J = 3.0 Hz, 1H), 7.38−7.44 (m, 2H), 7.34 (dd, J = 5.1, 3.0 Hz, 1H), 6.80 (d, J = 8.1 Hz, 1H), 6.45 (d, J = 8.1 Hz, 1H), 3.89 (t, J = 19.5 Hz, 1H).
^{13}C NMR (75 MHz, D_2O) δ 158.32, 150.32, 140.68, 139.50, 126.87, 126.04, 123.71, 109.30, 106.75, 51.31 (CH, t, J = 123.8 Hz).
^{31}P NMR (81 MHz, D_2O) δ 15.69.
HRMS: calcd for $C_{10}H_{11}N_2O_6P_2S$ m/z 348.9819 $(M - H^+)^-$; found m/z 349.0676.

Inhibitor **16c**. ^{1}H NMR (300 MHz, D_2O) δ 7.75 (d, J = 6.6 Hz, 2H), 7.49 (dd, J = 7.8, 7.8 Hz, 1H), 7.29−7.40 (m, 3H), 6.88 (d, J = 7.2 Hz, 1H), 6.55 (d, J = 8.4 Hz, 1H), 3.96 (t, J = 18.9 Hz, 1H).
^{13}C NMR (75 MHz, D_2O) δ 161.13, 157.33, 141.92, 141.29, 131.50, 131.31, 129.43, 112.28, 109.31, 53.78 (CH, t, J = 122.6 Hz).
^{31}P NMR (81 MHz, D_2O) δ 15.78.
HRMS: calcd for $C_{12}H_{13}N_2O_6P_2$ m/z 343.0254 $(M - H^+)^-$; found m/z 343.0259.

Inhibitor **16f**. ^{1}H NMR (300 MHz, D_2O) δ 8.13 (s, 1H), 8.09 (s, 1H), 7.63 (d, J = 5.9 Hz, 1H), 7.55 (d, J = 6.5 Hz, 1H), 7.44 (dd, J = 5.9, 5.9 Hz, 1H), 6.84 (d, J = 5.9 Hz, 1H), 6.43 (d, J = 6.5 Hz, 1H).
^{13}C NMR (75 MHz, D_2O) δ 159.13 (C), 156.24 (CH), 153.78 (C), 147.51 (C), 139.09 (C), 134.76 (CH), 130.27 (CH), 123.68 (CH), 123.25 (CH), 119.00 (CH), 113.47 (CH), 108.59 (C).
^{31}P NMR (81 MHz, D_2O) δ 16.86.
HRMS: calcd for $C_{13}H_{13}N_4O_6P_2$ m/z 383.0316 $(M - H^+)^-$; found m/z 383.0327.

Expression and Purification of Recombinant hFPPS. A plasmid encoding N-terminally His_6-tagged human FPPS (vector p11; SGC Oxford) was transformed into *E. coli* BL21(DE3) cells. The cells were induced overnight for hFPPS expression in the presence of 1 mM IPTG at 18 °C and lysed in a buffer containing 50 mM HEPES (pH 7.5), 500 mM NaCl, 10 mM β-mercaptoethanol, 5 mM imidazole, and 5% (v/v) glycerol. The lysate was cleared by centrifugation and passed through a Ni-NTA agarose column. Elution was carried out in an increasing imidazole gradient. The hFPPS containing fractions were pooled and applied to a Superdex 200 column, and the protein was eluted in high purity in a buffer containing 10 mM HEPES (pH 7.5), 500 mM NaCl, 10 mM β-mercaptoethanol, and 5% glycerol. The protein sample was concentrated to 12.5 mg/mL with a spin column concentrator.

In Vitro Inhibition Assay for hFPPS. The assay was based on a literature procedure with minor modifications.[15] All assays were run in triplicate using 40 ng of the human recombinant FPPS and 10 μM of each substrates, GPP and IPP (^{3}H-IPP, 3.33 mCi/mmol), in a final volume of 100 μL buffer containing 50 mM Tris at pH 7.7, 2 mM $MgCl_2$, 0.5 mM TCEP, and 20 μg/mL BSA. For the assays run with a 10 min preincubation period, the enzyme and inhibitor were incubated in the assay buffer in a volume of 80 μL at 37 °C for 10 min. After 10 min, the substrates were added to start the reaction and also bring the inhibitor and substrate to the desired final concentrations. For assays run without preincubation, the reaction was started with the addition

of enzyme to the mixture of inhibitor and the two substrates. After addition of all substrates, all assays were incubated at 37 °C for 20 min. Assays were terminated by the addition of 200 μL of HCl/methanol (1:4) and incubated for 10 min at 37 °C. The assay mixture was then extracted with 700 μL of ligroin (in order to separate reaction products from the unused substrate), and 300 μL of the ligroin upper phase was combined with 8 mL of scintillation cocktail. The radioactivity was then counted using a Beckman Coulter LS6500 liquid scintillation counter.

Reagents for Enzymatic Assay. Ligroin was purchased from Sigma Aldrich, liquid scintillation cocktail was purchased from MP Biomedicals: Ecolite (#882475), ^{3}H-IPP was purchased from American Radiolabeled Chemicals (ART 0377A: 1 mCi/mL, 60 Ci/mmol in 0.1 M Tris pH7.5), and unlabeled IPP and GPP were purchased from Isoprenoids, Lc. as their ammonium salts.

hFPPS Solution. The hFFPS enzyme was stored at −80 °C as a 2 μg/μL solution in the eluent buffer (50 mM HEPES at pH 7.5, 500 mM NaCl, 250 mM imidazole, 5% glycerol, and 0.5 mM TCEP).

IPP Solution. ^{3}H-IPP was diluted with IPP to a specific activity of 33 mCi/mmol and 100 μM concentration in 1 M Tris at pH 7.7. It was stored at −10 °C, warmed to 0 °C, and kept on ice during assay setup.

GPP Solution. GPP was dissolved and diluted to a 100 μM concentration in 1 M Tris at pH 7.7. It was stored at −10 °C, warmed to 0 °C, and kept on ice during assay setup.

Expression, Purification and in Vitro Assay of Recombinant hGGPPS. A plasmid encoding N-terminally His_6-tagged human GGPPS (vector pNIC28-Bsa4, SGC Oxford) was transformed into *E. coli* BL21(DE3) cells as previously reported.[31] The protocols described by Kavanagh and co-workers were used for both the purification and *in vitro* assay of hGGPPS.[31]

Cell Culture and Viability Assays. The JJN3 multiple myeloma cell line was obtained courtesy of Dr. Leif Bergsagel (Mayo Clinic, Scottsdale, AZ) and cultured in RPMI-1640 medium supplemented with 10% fetal bovine serum (Gibco BRL, Gaithesburg, Md) supplemented with 2 mM L-glumatime in a 5% CO_2 atmosphere at 37 °C. A dilution method was used to determine EC_{50} values for inhibition for each target compound; compounds were diluted in culture medium. Cells were seeded in 96 well plates at a density 10,000 cells per well and incubated for 2 h before the addition of 10 μL of compound at half-logarithmic dilutions from 100 nM to 333 μM with a fixed final volume. Plates were then incubated for 72 h at 37 °C in the presence 5% CO_2, following which an MTT, 4,5-dimethylthiazole-2-yl)-2,5- diphenyltetrazolium bromide reagent was used according to the manufacturer's documentation (Promega, Madison, WI). Plates were read at OD490 nM on a Dynex MRX microplate reader (Magellan Biosciences, Chelmsford MA). Results were analyzed to obtain dose−response curves and EC_{50} calculations using GraphPad PRISM, version 5 for MacIntosh (GraphPad Software, San Diego, CA).

Apoptosis in the Myeloma Cell Assay. To determine the ability of compound **13v** to induce MM cell lines to undergo apoptosis, cells were seeded at a density of 2 × 105/mL in medium supplemented with 10% FBS with increasing concentrations of **13v** or vehicle alone. Following a 48 h of incubation, apoptosis was determined by double staining with Annexin V and 7-AAD (BD Biosciences, Mississauga ON) according to the manufacturer's directions. Samples were analyzyed by FACScan analysis using CellQuest Software.

Western Blot Analysis for pERK Activity. RPMI8226 cells were serum starved overnight, then treated with 10% FBS with or without 100 μM YS-90 compound at 0 (serum starved alone), 10, and 20 min. Cells were then immediately washed with ice cold PBS/BSA, centrifuged, and resuspended in 1 mL of lysis buffer (10% Triton, 0.5% sodium deoxycholate, 0.1 N NaCl, 1 mM EDTA, 10 mM Na_2HPO_4, 10 mM phenylmethylsulfonyl fluoride (PMSF), 20 mM benzamidin, 1 mM leupeptin, and 0.025 U/mL of aprotinin). Equal amounts of proteins were run on an SDS−PAGE gel, then the separated proteins were electrotranferred to nitrocellulose membranes, and hybridized with either a polyclonal antibody to phospho ERK (phospho-p44/42 MAPK (ERK1/2) #9101, Cell Signaling Technology, Danvers MA) or total ERK (p44/41 MAPK (ERK1/2) #9102, Cell Signaling Technology). Following a wash, membranes were then exposed to HRP- conjugated secondary antibodies. Finally, membranes were washed with PBS/0.05% Tween 20, and immunoreactive proteins were detected by ECL, chemiluminescence (Amersham, Uppsala, Sweden).

Crystallization and X-ray Data Collection. Compound **13k** was prepared as a 200 mM stock solution in 100 mM Tris-HCl (pH 7.5) and $MgCl_2$ as a 200 mM aqueous solution. These solutions were added to the concentrated protein sample to give a final concentration of 2 mM compound **13k** as well as $MgCl_2$ and a final protein concentration of 10 mg/mL. This protein/inhibitor mix was incubated on ice for 30 min, after which time the precipitate formed in the sample was removed by centrifugation. Crystals were grown at 22 °C in a sitting drop prepared by mixing 1 μL of the protein mix and 100 μL of the reservoir solution, which contained 100 mM sodium acetate (pH 4.6) and 30% (v/v) PEG 300. Diffraction data were collected from a single crystal at the Canadian Light Source (CLS), Saskatoon, SK, as 0.8° oscillation images (224 frames).

Data Processing and Refinement. The collected diffraction images were indexed, integrated, and scaled with HKL2000.[35] The initial phase was calculated by molecular replacement with the program PHASER,[36] with a previously determined hFPPS structure (PDB code: 3N46) as a search model. The structure model of the hFPPS/**13k** complex was further improved through iterative rounds of manual model building with COOT[37] and automated refinement with PHENIX[38] and REFMAC5.[39] Data collection and refinement statistics are summarized in Table 4. The refined structure of our hFPPS/**13k** complex has been deposited into the Protein Data Bank with the entry code 4DEM.

Table 4. Data Collection and Refinement Statistics

Data Collection	
wavelength (Å)	0.97949
space group	$P4_12_12$
unit cell dimension (Å)	$a = b = 111.23$, $c = 67.72$
resolution range (Å)	50.0−1.85 (1.88−1.85)[a]
redundancy	14.3 (14.0)
completeness (%)	99.9 (100)
$I/\sigma(I)$	50.43 (8.0)
R_{merge}	0.048 (0.391)
Refinement	
no. of reflections	34,866
R_{work}/R_{free}	0.174/0.202
no. of water molecules	221
rms Deviations	
bond length (Å)	0.026
bond angle (deg)	1.7

[a]Values in parentheses are for the highest resolution shell.

Computational studies. All calculations were performed using the Schrödinger suite: Maestro (version 9.0), Glide (version 5.5), ConfGen, (version 2.1), LigPrep, (version 2.3), and QikProp (version 3.2) (Schrödinger, LLC, New York, NY, 2009).[32,33] All images were generated using PyMol (www.pymol.org).

Protein Preparation for Docking. All crystal structures were downloaded directly from the PDB database and prepared using the Protein Preparation Wizard feature using standard parameters. The proteins were overlapped with the secondary structure alignment tool, using the hinge-region between Helix I and II as reference.

Docking Grid Generation. Three grids were generated using standard parameters, encompassing the two active site subpockets (i.e., binding sites of IPP and GPP) from the hFPPS/**2** binary complex (PDB ID: 1YV5) and the hFPPS/IPP/**1** ternary complex (PDB ID: 1ZW5) as well as the allosteric site from the hFPPS/IPP/FBS-04 ternary complex (PDB ID: 3N45).

For all protein structures, the "rotatable OH-bonds" feature was enabled for the residues listed below:

(1) 1YV5 (hFPPS/**2**): Thr 77, Thr 215, Tyr 218, and Ser 219
2) 1ZW5 (hFPPS/IPP/**1**): Thr 215, Tyr 218, and Ser 219
3) 3N45 (hFPPS/**1**/FBS-04): Thr 63, Thr 201, Tyr 204, and Ser 205

Docking. All bisphosphonates were docked in their fully ionized (tetra-anion) forms, and conformation libraries were generated using ConfGen (using the parameters "standard" and "intermediate"; only input minimization) followed by LigPrep (retain original ionization state; output tautomers). Docking was performed with Glide (5.5), flexible docking, extra precision (XP-mode),[34] and standard parameters.

Library design was guided by docking virtual molecules in to the fully closed hFPPS active site (PDB ID: 1ZW5). Previously, we validated our *in silico* model using a library of structurally related compounds to those reported herein.[23] Compounds expected to bind favorably into the hFPPS active site, as well as molecules predicted to bind poorly or not at all, were synthesized and tested in the *in vitro* inhibition assay.

Analysis. All output structures were visually inspected, and poses that did not have the bisphosphonate moiety properly aligned to the Mg^{2+}-triad (as compared to the crystal structures of 1YV5 and 1ZW5) were rejected. In general, high conformational consistency of the output poses was observed. For example, for 20 docked poses of inhibitor **13k**, bound *in silico* to the fully closed active site (PDB ID 1ZW5), very high consistency was observed for the binding of the bisphosphonate moiety and the 2-aminopyridine core (Supporting Information,Figure SI-1). The highest variability observed was in the binding orientations of the isopropyl side chain with a maximum range of 1.7 Å. In general, these studies suggested that the pyridine core of **13k** would bind in a ~90° angle relative to the enzyme-bound heterocyclic side chain of **1**, placing the 4-isopropoxyphenyl moiety into the IPP subpocket, suggesting that the larger side chain of **13k** would forbid binding in the GPP subpocket alone without imposing significant conformational rearrangements to the protein structure.

■ ASSOCIATED CONTENT

Supporting Information

NMR spectra of key compounds **8c**, **8f**, **9a**, **9c**, **8f**, **13a**, **13c**, **13f**, **13j**, **13k**, **13l**, **13o**, **13p**, **13u**, **13y**, **13v**, **13y**, and **13z**; examples of homogeneity data for key inhibitors at the bisphosphonate tetraester stage and the final bisphosphonates; and some experimental details on the docking studies and the ^{1}H NMR line broadening experiments. This material is available free of charge via the Internet at http://pubs.acs.org.

■ AUTHOR INFORMATION

Corresponding Author

*Phone: 514-398-3638. Fax: 514-398-3797. E-mail: Youla.tsantrizos@mcgill.ca.

Notes

The authors declare no competing financial interest.

■ ACKNOWLEDGMENTS

We are grateful to Dr. Tara Sprules for assistance with the setup of the ^{1}H NMR line broadening experiments, which were acquired on a 500 MHz NMR instrument at the Québec/Eastern Canada High Field NMR Facility, supported by the Natural Sciences and Engineering Research Council of Canada (NSERC), the Canada Foundation for Innovation (CFI), the Québec ministère de la recherche en science et technologie (FQRNT), and McGill University. Financial support for this work was provided by McGill University, NSERC and FQRNT (to Y.S.T.). We also thank the Canadian Institute of Health Research (CIHR; to Y.-S.L. and J.W.D.S.), the Ministry of Education of Taiwan (to Y.-S.L.), and the Groupe de Recherche Axé sur la Structure des Protéines (GRASP; to J.W.D.S.).

■ ABBREVIATIONS USED

hFPPS, human farnesyl pyrophosphate synthase; hGGPPS, human geranylgeranyl pyrophosphate synthase; DMAPP, dimethylallyl pyrophosphate; IPP, isopentenyl pyrophosphate; GPP, geranyl pyrophosphate; FPP, farnesyl pyrophosphate; GGPP, geranylgeranyl pyrophosphate; *N*-BPs, nitrogen-containing bisphosphonates; MM, multiple myeloma; GTPases, small guanine triphosphate binding proteins; ANT, mitochondrial adenine nucleotide translocase; IFNγ, interferon-gamma; TNFα, tumor necrosis factor-alpha; ERK, extracellular-signal regulated kinase 1/2; MAPK, p42/p44 mitogen activated protein kinase; hDPPS, human decaprenyl diphosphate synthase; hSQS, human squalene synthase; ApppI, derivative 1-adenosin-5′-yl ester 3-(3-methylbut-3-enyl) triphosphoric acid

■ REFERENCES

(1) Berndt, N.; Hamilton, A. D.; Sebti, S. M. Targeting protein prenylation for cancer theraphy. *Nature Rev.* **2011**, *11*, 775−791.
(2) Chapman, M. A.; Lawrence, M. S.; Keats, J. J.; Cibulskis, K.; Sougnez, C.; Schinzel, A. C.; Harview, C. L.; Brunet, J. P.; Ahmann, G. J.; Adli, M.; Anderson, K. C.; Ardlie, K. G.; Auclair, D.; Baker, A.; Bergsagel, P. L.; Bernstein, B. E.; Drier, Y.; Fonseca, R.; Gabriel, S. B.; Hofmeister, C. C.; Jagannath, S.; Jakubowiak, A. J.; Krishnan, A.; Levy, J.; Liefeld, T.; Lonial, S.; Mahan, S.; Mfuko, B.; Monti, S.; Perkins, L. M.; Onofrio, R.; Pugh, T. J.; Rajkumar, S. V.; Ramos, A. H.; Siegel, D. S.; Sivachenko, A.; Stewart, A. K.; Trudel, S.; Vij, R.; Voet, D.; Winckler, W.; Zimmerman, T.; Carpten, J.; Trent, J.; Hahn, W. C.; Garraway, L. A.; Meyerson, M.; Lander, E. S.; Getz, G.; Golub, T. R. Initial genome sequencing and analysis of multiple myeloma. *Nature* **2011**, *471*, 467−472.
(3) Rondeau, J.-M.; Bitsch, F.; Bourgier, E.; Geiser, M.; Hemmig, R.; Kroemer, M.; Lehmann, S.; Ramage, P.; Rieffel, S.; Strauss, A.; Green, J. R.; Jahnke, W. Structural basis for the exceptional *in vivo* efficacy of bisphosphonate drugs. *ChemMedChem* **2006**, *1*, 267−273.
(4) Kavanagh, K. L.; Guo, K.; Dunford, J. E.; Wu, X.; Knapp, S.; Ebetino, F. H.; Rogers, M. J.; Russell, R. G. G.; Oppermann, U. The molecular mechanism of nitrogen-containing bisphosphonates as antiosteoporosis drugs. *Proc. Natl. Acad. Sci. U.S.A.* **2006**, *103*, 7829−7834.
(5) Review: Dunford, J. E. Molecular targets of the nitrogen containing bisphosphonates: the molecular pharmacology of prenyl synthase inhibition. *Curr. Pharm. Des.* **2010**, *16*, 2961−2969.
(6) Morgan, G. J.; Davies, F. E.; Gregory, W. M.; Cocks, K.; Bell, S. E.; Szubert, A. J.; Navarro-Coy, N.; Drayson, M. T.; Owen, R. G.; Feyler, S.; Ashcroft, A. J.; Ross, F.; Byrne, J.; Roddie, H.; Rudin, C.; Cook, G.; Jackson, G. H.; Child, J. A. First-line treatment with zoledronic acid as compared with clodronic acid in multiple myeloma (MRC Myeloma IX): a randomised controlled trial. *Lancet* **2010**, *376*, 1989.
(7) Mönkkönen, H.; Auriola, S.; Lehenkari, P.; Kellinsalmi, M.; Hassinen, I. E.; Vepsäläinen, J.; Mönkkönen, J. A new endogenous ATP analog (ApppI) inhibits the mitochondrial adenine nucleotide translocase (ANT) and is responsible for the apoptosis induced by nitrogen-containing bisphosphonates. *Br. J. Pharmacol.* **2006**, *147*, 437−445.
(8) Mitrofan, L. M.; Pelkonen, J.; Mönkkönen, J. The level ofATP analogs and isopentenyl pyrophosphate correlates with zoledronic acid-induced apoptosis in cancer cells in vitro. *Bone* **2009**, *45*, 1153−1160.
(9) Review: Morita, C. T.; Jin, C.; Sarikonda, G.; Wang, H. Nonpeptide antigens, presentation mechanisms, and immunological

memory of human Vγ2Vδ2 T cells: discriminating friends from foe through the recognition of prenyl pyrophosphate antigens. *Immunol. Rev.* **2007**, *215*, 59−76.
(10) Zhang, Y.; Leon, A.; Song, Y.; Studer, D.; Haase, C.; Koscielski, L. A.; Oldfield, E. Activity of Nitrogen-containing and non-nitrogen-containing bisphosphonates on tumor cell lines. *J. Med. Chem.* **2006**, *49*, 5804−5814.
(11) Ezra, A.; Hoffma, A.; Breuer, E.; Alferiev, I. S.; Mönkkönen, J.; Hanany-Rozen, N.El; Weiss, G.; Stepensky, D.; Gati, I.; Cohen, H.; Törmä, S.; Amidon, G. L.; Golomb, G. A peptide prodrug approach for improving bisphosphonate oral absorption. *J. Med. Chem.* **2000**, *43*, 3641−3652.
(12) Shmeeda, H.; Amitay, Y.; Gorin, J.; Tsemach, D.; Mak, L.; Ogorka, J.; Kumar, S.; Zhang, J. A.; Gabizon, A. Delivery of zoledronic acid encapsulated in folate-targeted liposome results in potent *in vitro* cytotoxic activity on tumor cells. *J. Controlled Release* **2010**, *146*, 76−83.
(13) Dunford, J. E.; Thompson, K.; Coxon, F. P.; Luckma, S. P.; Hahn, F. M.; Poulter, C. D.; Ebetino, F. H.; Rogers, M. J. Structure-activity relationship for inhibition of farnesyl diphosphate synthase in vitro and inhibition of bone resorption in vivo by nitrogen-containing bisphosphonates. *J. Pharmacol. Exp. Ther.* **2001**, *296*, 235−242.
(14) Marma, M. S.; Xia, Z.; Stewart, C.; Coxon, F.; Dunford, J. E.; Baron, R.; Kashemirov, B. A.; Ebetino, F. H.; Triffitt, J. T.; Russell, G. G.; McKenna, C. E. Synthesis and biological evaluation of α-halogenated bisphosphonate and phosphonocarboxylate analogues of risedronate. *J. Med. Chem.* **2007**, *50*, 5967−5975.
(15) Dunford, J. E.; Kwaasi, A. A.; Rogers, M. J.; Barnett, B. L.; Ebetino, F. H.; Russell, R. G. G.; Oppermann, U.; Kavanagh, K. L. Structure-activity relationship among the nitrogen containing bisphosphonates in clinical use and other analogues: time-dependent inhibition of human farnesyl pyrophosphate synthase. *J. Med. Chem.* **2008**, *51*, 2187−2195.
(16) Zhang, Y.; Cao, R.; Yin, F.; Hudock, M. P.; Guo, R.-T.; Krysiak, K.; Mukherjee, S.; Gao, Y.-G.; Robinson, H.; Song, Y.; No, J. H.; Bergan, K.; Leon, A.; Cass, L.; Goddard, A.; Chang, T.-K.; Lin, F.-Y.; Van Beek, E.; Papapoulos, S.; Wang, A.H.-J.; Kubo, T.; Ochi, M.; Mukkamala, D.; Oldfield, E. Lipophilic bisphosphonates as dual farnesyl/geranylgeranyl diphosphate synthase inhibitors: an X-ray and NMR investigation. *J. Am. Chem. Soc.* **2009**, *131*, 5153−5162.
(17) Wiemer, A. J.; Tong, H.; Swanson, K. M.; Hohl, R. J. Digeranyl bisphosphonate inhibits geranylgeranyl pyrophosphate synthase. *Biochem. Biophys. Res. Commun.* **2007**, *353*, 921−925.
(18) Simoni, D.; Gebbia, N.; Invidiata, F. P.; Eleopra, M.; Marchetti, P.; Rondanin, R.; Baruchello, R.; Provera, S.; Marchioro, C.; Tolomeo, M.; Marinelli, L.; Limongelli, V.; Novellino, E.; Kwaasi, A.; Dunford, J.; Buccheri, S.; Caccamo, N.; Dieli, F. Design, synthesis, and biological evaluation of novel aminobisphosphonates possessing an in vivo antitumor activity through a γδ-T lymphocyte-mediated activation mechanism. *J. Med. Chem.* **2008**, *51*, 6800−6807.
(19) Zhang, Y.; Cao, R.; Yin, F.; Lin, F.-Y.; Wang, H.; Krysiak, K.; No, J.-H.; Mukkamala, D.; Houlihan, K.; Li, J.; Morita, C. T.; Oldfield, E. Lipophilic pyridinium bisphosphonates: potent γδ T cell stimulators. *Angrew. Chem. Int. Ed.* **2010**, *49*, 1136−1138.
(20) Lolli, M. L.; Rolando, B.; Tosco, P.; Chaurasia, S.; Di Stilo, A.; Lazzarato, L.; Gorassini, E.; Ferracini, R.; Oliaro-Bosso, S.; Fruttero, R.; Gasco, A. Synthesis and preliminary pharmacological characterisation of a new class of nitrogen-containing bisphosphonates (N-BPs). *Bioorg. Med. Chem.* **2010**, *18*, 2428−2438.
(21) Wasko, B. M.; Smits, J. P.; Shull, L. W.; Wiemer, D. F.; Hohl, R. J. A novel bisphosphonate inhibitor of squalene synthase combined with a statin or a nitrogenous bisphosphonate in vitro. *J. Lipid. Res.* **2011**, *52*, 1957−1964.
(22) Jahnke, W.; Rondeau, J.-M.; Cotesta, S.; Marzinzik, A.; Pellé, X.; Geiser, M.; Strauss, A.; Götte, M.; Bitsch, F.; Hemmig, R.; Henry, C.; Lehmann, S.; Glickman, J. F.; Roddy, T. P.; Stout, S. J.; Green, J. R. Allosteric non-bisphosphonate FPPS inhibitors identified by fragment-based discovery. *Nature Chem. Biol* **2010**, *6*, 660−666.
(23) De Schutter, J. W.; Zaretsky, S.; Welbourn, S.; Pause, A.; Tsantrizos, Y. S. Novel bisphosphonate inhibitors of the human farnesyl pyrophosphate synthase. *Biorg. Med. Chem. Lett.* **2010**, *20*, 5781−5786.
(24) Guram, A. S.; Wang, X.; Bunel, E. E.; Faul, M. M.; Larsen, R. D.; Martinelli, M. J. New catalysts for Suzuki−Miyaura coupling reactions of heteroatom-substituted heteroaryl chlorides. *J. Org. Chem.* **2007**, *72*, 5104−5112.
(25) Fleckenstein, C. A.; Plenio, H. Highly efficient Suzuki−Miyaura coupling of heterocyclic substrates through rational reaction design. *Chem.—Eur. J.* **2008**, *14*, 4267−4279.
(26) Matczak-Jon, E.; Ślepokura, K.; Kafarski, P. Solid state and solution behaviour of *N*-(2-pyridyl)- and *N*-(4-methyl-2-pyridyl)-aminomethane-1,1-diphosphonic acids. *J. Mol. Struct.* **2006**, *782*, 81−93.
(27) Tarshis, L. C.; Proteau, P. J.; Kellogg, B. A.; Sacchettini, J. C.; Poulter, C. D. Regulation of product chain length by isoprenyl diphosphate synthase. *Proc. Natl. Acad. Sci. U.S.A.* **1996**, *93*, 15018−15023.
(28) Martin, M. B.; Arnold, W.; Heath, H. T. III; Urbina, J. A.; Oldfield, E. Nitrogen-containing bisphosphonates as carbocation transition state analogs for isoprenoid biosynthesis. *Biochem. Biophys. Res. Commun.* **1999**, *263*, 754−758.
(29) Räikkönen, J.; Taskinen, M.; Dunford, J. E.; Mönkkönen, H.; Auriola, S.; Mönkkönen, J. Correlation between time-dependent inhibition of human farnesyl pyrophosphate synthase and blockade of mevalonate pathway by nitrogen-containing bisphosphonate in cultured cells. *Biochem. Biophys. Res. Commun.* **2011**, *407*, 663−667.
(30) Song, L.; Poulter, C. D. Yeast farnesyl-diphosphate synthase: site-directed mutagenesis of residues in highly conserved prenyltransferase domains I and II. *Proc. Natl. Acad. Sci. U.S.A.* **1994**, *91*, 3044−3048.
(31) Kavanagh, K. L.; Dunford, J. E.; Bunkoczi, G.; Russell, R. G. G.; Oppermann, U. The Crystal structure of human geranylgeranyl pyrophosphate synthase reveals a novel hexameric arrangement and inhibitory product binding. *J. Biol. Chem.* **2006**, *281*, 22004−22012.
(32) Halgren, T. A.; Murphy, R. B.; Friesner, R. A.; Beard, H. S.; Frye, L. L.; Pollard, W. T.; Banks, J. L. Glide: a new approach for rapid, accurate docking and scoring. 2. Enrichment factors in database screening. *J. Med. Chem.* **2004**, *47*, 1750−1759.
(33) Friesner, R. A.; Banks, J. L.; Murphy, R. B.; Halgren, T. A.; Klicic, J. J.; Mainz, D. T.; Repasky, M. P.; Knol, E. H.; Shelley, M.; Perry, J. K.; Shaw, D. E.; Francis, P.; Shenkin, P. S. Glide: a new approach for rapid, accurate docking and scoring. 1. Method and assessment of docking accuracy. *J. Med. Chem.* **2004**, *47*, 1739−1749.
(34) Friesner, R. A.; Murphy, R. B.; Repasky, M. P.; Frye, L. L.; Greenwood, J. R.; Halgren, T. A.; Sanschagrin, P. C.; Mainz, D. T. Extra precision Glide: docking and scoring incorporating a model of hydrophobic enclosure for protein−ligand complexes. *J. Med. Chem.* **2006**, *49*, 6177−6196.
(35) Otwinowski, Z.; Minor, W. Processing of X-ray Diffraction Data Collected in Oscillation mode. In *Methods in Enzymology*; Carter, C. W., Jr., Sweet, R. M., Eds.; Elsevier: New York, **1997**; Vol. *276*, Macromolecular Crystallography, Part A, pp 307−326.
(36) McCoy, A. J.; Grosse-Kunstleve, R. W.; Adams, P. D.; Winn, M. D.; Storoni, L. C.; Read, R. J. Phaser crystallographic software. *J. Appl. Crystallogr.* **2007**, *40*, 658−674.
(37) Emsley, P.; Cowtan, K. Coot: model-building tools for molecular graphics. *Acta Crystallogr., Sect. D* **2004**, *60*, 2126−2132.
(38) Adams, P. D.; Afonine, P. V.; Bunkoczi, G.; Chen, V. B.; Davis, I. W.; Echols, N.; Headd, J. J.; Hung, L.-W.; Kapral, G. J.; Grosse-Kunstleve, R. W.; McCoy, A. J.; Mriarty, N. W.; Oeffner, R.; Read, R. J.; Richardson, D. C.; Richardson, J. S.; Terwilliger, T. C.; Zwart, P. H. A comprehensive Python-based system for macromolecular structure solution. *Acta Crystallogr., Sect. D* **2010**, *66*, 213−221.
(39) Vagin, A. A.; Steiner, R. S.; Lebedev, A. A.; Potterton, L.; McNicholas, S.; Long, F.; Murshudov, G. N. REFMAC5 dictionary: organization of prior chemical knowledge and guidelines for its use. *Acta Crystallogr., Sect. D* **2004**, *60*, 2284−2295.

(40) Heim, R.; Lucas, S.; Grombein, C. M.; Ries, C.; Schewe, K. E.; Negri, M.; Müller-Vieira, U.; Birk, B.; Hartmann, R. W. Overcoming undesirable CYP1A2 inhibition of pyridylnaphthalene-type aldosterone synthase inhibitors: influence of heteroaryl derivatization on potency and selectivity. *J. Med. Chem.* **2008**, *51*, 5064−5074.